# Energy-Based Liquefaction Triggering Model

 $\textbf{Article} \ \textit{in} \ \mathsf{Journal} \ \mathsf{of} \ \mathsf{Geotechnical} \ \mathsf{and} \ \mathsf{Geoenvironmental} \ \mathsf{Engineering} \cdot \mathsf{November} \ \mathsf{2023}$ 

DOI: 10.1061/JGGEFK.GTENG-11402

CITATION

1

READS 342

4 authors, including:



#### Kristin Ulmer

Southwest Research Institute

14 PUBLICATIONS 45 CITATIONS

SEE PROFILE



#### Adrian Rodriguez-Marek

Virginia Tech (Virginia Polytechnic Institute and State University)

149 PUBLICATIONS 4,010 CITATIONS

SEE PROFILE



#### Russell A Green

Virginia Tech (Virginia Polytechnic Institute and State University)

232 PUBLICATIONS 4,102 CITATIONS

SEE PROFILE





# **Energy-Based Liquefaction Triggering Model**

K. J. Ulmer, A.M.ASCE<sup>1</sup>; R. A. Green, F.ASCE<sup>2</sup>; A. Rodriguez-Marek, M.ASCE<sup>3</sup>; and J. K. Mitchell, Hon.M.ASCE<sup>4</sup>

**Abstract:** The most commonly used approach for evaluating liquefaction triggering is via stress-based simplified models. Proposed herein is a model for evaluating liquefaction triggering where the imposed loading and ability of the soil to resist liquefaction are quantified in terms of normalized dissipated energy per unit volume of soil  $(\Delta W/\sigma'_{vo})$ , computed within a total stress framework. The proposed model overcomes limitations of many previously proposed energy-based triggering models. Additionally, the proposed energy-based model unites concepts from both stress-based and strain-based procedures, overcoming some of their limitations, and in its simplified form is implemented similarly to the simplified stress-based models. An updated field case history database is used to develop probabilistic limit-state curves. These limit-state curves express  $\Delta W/\sigma'_{vo}$  required to trigger liquefaction as a function of corrected cone penetration test tip resistance  $(q_{c1Ncs})$  for different probabilities of liquefaction  $(P_L)$  and have comparable predictive abilities to stress-based limit-state curves in terms of number of correct predictions for the cases analyzed. However, because dissipated energy is a scalar quantity, multidirectional shaking and other effects such as soil–structure interaction, nonvertical wave fields, and topographic site effects can readily be accounted for. Additionally, the applicability of the proposed triggering curve is not limited to earthquake loading but, rather, can be used in relation to other sources of vibrations (e.g., construction vibrations and explosive loading, among others). **DOI: 10.1061/JGGEFK.GTENG-11402.** © 2023 American Society of Civil Engineers.

Author keywords: Liquefaction; Liquefaction triggering; Energy-based triggering model; Limit-state curves; Maximum likelihood.

#### Introduction

The most commonly used approach for evaluating liquefaction triggering is via simplified stress-based models, where the imposed loading and the ability of the soil to resist liquefaction are expressed in terms of cyclic shear stress and resistance ratios for a set of reference conditions. However, the simplified stress-based framework has some drawbacks, some of which result from the oversimplification of the imposed loading and the imposed reference conditions. Specifically, the imposed loading is expressed in terms of normalized cyclic stress ratio (CSR\*), which can be divided into components that represent the amplitude and duration of the loading. The amplitude of the loading is proportional to the peak horizontal acceleration at the ground surface ( $a_{\rm max}$ ), and the duration of the loading is expressed in terms of the magnitude scaling factor (MSF).

In turn, MSF is a function of the number of equivalent loading cycles  $(n_{eq,M})$  for ground motions from an earthquake with moment magnitude (M) relative to  $n_{eq,M}$  for a moment magnitude 7.5 (M7.5) earthquake,  $n_{eq,M7.5}$  (i.e., the reference event). This

Note. This manuscript was submitted on October 7, 2022; approved on July 6, 2023; published online on September 6, 2023. Discussion period open until February 6, 2024; separate discussions must be submitted for individual papers. This paper is part of the *Journal of Geotechnical and Geoenvironmental Engineering*, © ASCE, ISSN 1090-0241.

simplification of the characteristics of the imposed loading makes the stress-based approach attractive because of its relative ease of implementation, but to some extent, it inherently limits the implementation scalability of the procedure, particularly in terms of duration of shaking, and limits the applicability of the procedure exclusively to earthquake loading. In this context, implementation scalability refers to the ability of the procedure to be implemented using refined estimates of the imposed loading and/or the ability of the soil to resist liquefaction triggering determined from numerical and/or laboratory studies. Quantifying ground motion duration in terms of MSF makes it difficult to apply the procedure to evaluate liquefaction due to nonearthquake vibrations (e.g., construction vibrations).

The characteristics of earthquake motions range widely, even for motions having similar values of  $a_{\text{max}}$  and M. As a result, alternative intensity measures (IM) to CSR\* have been proposed for quantifying the imposed loading for evaluating liquefaction triggering that better capture the characteristics of earthquake shaking. These include Arias intensity (e.g., Kayen and Mitchell 1997), cumulative absolute velocity (e.g., Kramer and Mitchell 2006), and other more direct measures of the energy associated with the imposed loading on the soil [e.g., dissipated energy (Berrill and Davis 1985)]. However, as elaborated upon subsequently in this paper, these alternative IMs and associated triggering models have their own shortcomings, including the introduction of erroneous variable dependencies, inconsistencies in the quantification of the imposed loading in a total stress framework and the ability of the soil to resist liquefaction in an effective stress framework, large uncertainty associated with predicting the IMs, and more pronounced issues with implementation scalability than the simplified stressbased procedure that they were developed to replace.

This paper proposes an energy-based liquefaction triggering model that quantifies the imposed loading and ability of the soil to resist liquefaction in terms of normalized dissipated energy per unit volume of soil, both computed within a total stress framework. Dissipated energy better captures the characteristics of

<sup>&</sup>lt;sup>1</sup>Research Engineer, Dept. of Geosciences and Engineering, Southwest Research Institute, San Antonio, TX 78238. ORCID: https://orcid.org/0000-0001-8696-7447. Email: kulmer@swri.org

<sup>&</sup>lt;sup>2</sup>Professor, Dept. of Civil and Environmental Engineering, Virginia Tech, Blacksburg, VA 24061 (corresponding author). ORCID: https://orcid.org/0000-0002-5648-2331. Email: rugreen@vt.edu

<sup>&</sup>lt;sup>3</sup>Professor, Dept. of Civil and Environmental Engineering, Virginia Tech, Blacksburg, VA 24061. ORCID: https://orcid.org/0000-0002-8384-4721. Email: adrianrm@vt.edu

<sup>&</sup>lt;sup>4</sup>University Distinguished Professor Emeritus, Dept. of Civil and Environmental Engineering, Virginia Tech, Blacksburg, VA 24061. Email: jkm@vt.edu

ground motions than CSR\* and has been shown to correlate well with excess pore-water pressure generation. From a mechanics perspective, the correlation of dissipated energy and excess pore-water pressure generation is expected because the predominant mechanism for energy dissipation in the soil is frictional, indicating relative movements of soil particles (e.g., Green 2001; Polito et al. 2013). This relative movement of soil particles is also the mechanism for excess pore-water generation. Furthermore, because dissipated energy is a scalar quantity, multidirectional shaking and other effects such as soil–structure interaction, nonvertical wave fields, and topographic site effects can readily be accounted for (e.g., Ostadan et al. 1998).

In its simplified form, the implementation of the proposed energy-based model is similar to the stress-based simplified models. However, implementation of the procedure is scalable, in that refined estimates of the loading or ability of the soil to resist liquefaction can be made via numerical site response analyses and/or laboratory testing. Such refinements are allowed as long as consistency is maintained in how the simplified form of the proposed energy-based model was developed and the refined estimates of the loading and ability of the soil to resist liquefaction are made (e.g., equivalent linear numerical analyses using the same shear modulus reduction and damping curves). Additionally, similar to the stress-based simplified models, the ability of the soil to resist liquefaction is derived from field case histories and correlated to in situ test metrics (i.e., normalized cone penetration test (CPT) tip resistance,  $q_{c1Ncs}$ ). This avoids issues regarding the representativeness of laboratory test data from reconstituted samples to in situ soil fabric and the need for correlations relating the relative density  $(D_r)$  of laboratory specimens to in situ test metrics. Finally, because normalized dissipated energy is a comprehensive and versatile IM, the applicability of the proposed triggering curve is not limited to earthquake loading but, rather, can be used in relation to other sources of vibrations (e.g., construction vibrations and explosive loading, among others).

In the following, background information regarding energy-based liquefaction triggering models and associated shortcomings is presented, followed by specifics of the proposed energy-based model. Toward the development of the triggering curve, modifications made to an existing liquefaction field case history database and how the case histories were analyzed to develop probabilistic limit-state curves are detailed. The implementation scalability and applicability of the proposed model are then discussed, as well as comparisons of the proposed energy-based framework with that of simplified stress-based models.

# **Background**

Development of energy-based methods for evaluating liquefaction began in the 1970s as an alternative to stress-based procedures (e.g., Nemat-Nasser and Shokooh 1979). Since then, liquefaction triggering models that use varying IMs have been broadly classified as energy-based procedures, to include models based on IMs such as Arias intensity ( $I_A$ ), cumulative absolute velocity (CAV), elastic strain energy, and energy dissipated per unit volume of soil ( $\Delta W$ ). Although there are merits and shortcomings with any given IM, the authors contend that  $\Delta W$  offers advantages over other IMs, with few drawbacks. The reason for this is that both the generation of excess pore pressures and energy dissipation result from the breakdown in the soil skeleton. As a result, dissipated energy in soil can be directly correlated to the generation of excess pore pressures throughout the loading and deformation process (e.g., Nemat-Nasser and Shokooh 1979; Simcock et al. 1983;

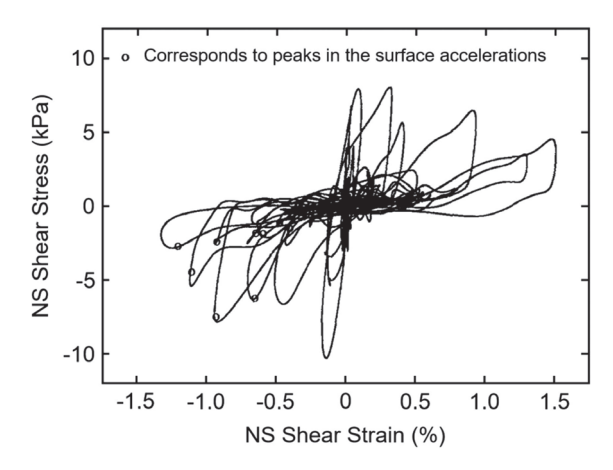


**Fig. 1.** Shear stress—shear strain hysteresis loops at a depth of 2.9 m in the Imperial Valley Wildlife Site profile for the 1987 M6.6 Superstitions Hills earthquake. (Reprinted from Zeghal and Elgamal 1994, © ASCE.)

Berrill and Davis 1985; Figueroa et al. 1994; Green et al. 2000; Davis and Berrill 2001; Jafarian et al. 2012; Polito et al. 2008; Kokusho and Kaneko 2018; Kokusho and Tanimoto 2021; among many others). Additionally, in its simplified form, the predictive variables for estimating  $\Delta W$  are similar to those used to compute the CSR\*; hence all the advances that have been made in estimating the predictive variables for CSR\* can be directly leveraged in predicting  $\Delta W$ .

The energy dissipated per unit volume of soil  $(\Delta W)$  is the difference between the shear strain energy input during the loading phase of a cycle and the elastic shear strain energy returned during the unloading phase of the cycle. Accordingly,  $\Delta W$  can be computed as the cumulative area bound by the shear stress—shear strain hysteresis loops such as those shown in Fig. 1.

As such,  $\Delta W$  reflects the amplitude and duration of the motion, to include the variation of the amplitude of the motion over the duration of shaking, as well as the element-level soil response to the shaking.  $\Delta W$  fundamentally differs from other, less direct, measures of ground motion energy (e.g., Arias intensity  $I_A$  and CAV).  $I_A$  and CAV are proportional to the square of ground acceleration and the absolute value of the ground velocity, respectively, integrated over the duration of the shaking. Because  $I_A$  and CAV are computed as integrals over time, they inherently introduce an erroneous dependency on ground motion frequency into the liquefaction models, conflating profile and soil element responses (Green and Mitchell 2003); this is elaborated on in the "Discussion" section of this paper. In contrast,  $\Delta W$  is computed by integrating the imposed shear stress over the induced shear strain in a soil element to quantify the loading on an element of soil, circumventing the frequency-dependency issue and the conflagration of profile and soil element responses.

A final, but important consideration, is that liquefaction is inherently a strain phenomenon (e.g., Martin et al. 1975; Dobry et al. 1982); however, simplified strain-based procedures (e.g., Dobry et al. 1982) have issues with the proper estimation of amplitude of the induced shear strain and the ground motion duration (Rodriguez-Arriaga and Green 2018; Green and Rodriguez-Arriaga 2019). The use of  $\Delta W$  as an IM merges aspects of the simplified stress- and strain-based liquefaction triggering concepts into one model, with the advantage that the use of  $\Delta W$  as the IM overcomes issues with quantifying the ground motion characteristics in terms of shear strain required by the simplified strain-based procedures.

#### **Energy-Based IM**

The authors propose using  $\Delta W$  computed within a total stress framework for their IM, where  $\Delta W$  is computed by integrating the imposed shear stress over the induced shear strain in a soil element for the duration of earthquake shaking. However, in the spirit of implementation scalability,  $\Delta W$  can be estimated via a simplified approach. Toward this end, the ground motions parameters that are used in simplified stress-based liquefaction triggering models (i.e.,  $a_{\max}$  and  $n_{eq,M}$ ) are used in conjunction with soil stiffness and shear modulus reduction and damping (MRD) curves for the soil (e.g., Ishibashi and Zhang 1993; Darendeli 2001) to estimate  $\Delta W$ . Specifically,  $a_{\max}$  and the MRD curves are used to estimate the dissipated energy in one equivalent cycle ( $\Delta W_{1,eq}$ ). An equation to estimate  $\Delta W_{1,eq}$  can be derived in terms of the damping ratio for a viscous material (D) (Jacobsen 1930) as follows:

$$D = \frac{\Delta W_{1,eq}}{4\pi W_{\text{stored}}} \tag{1}$$

where  $W_{\rm stored}=$  elastic stored energy, equal to  $0.5\cdot \tau\cdot \gamma$ , where  $\tau$  and  $\gamma$  are the imposed shear stress and the induced shear strain, respectively. Rearranging terms and letting  $\tau=\tau_{\rm avg}$ , where  $\tau_{\rm avg}$  is the representative (or average) amplitude of shear stress of the imposed loading and  $\gamma=\gamma_c=\tau_{\rm avg}/G_{\gamma c}$ , where  $G_{\gamma c}$  is the secant shear modulus corresponding to  $\gamma_c$ , the equation for  $\Delta W_{1,eq}$  then becomes

$$\Delta W_{1,eq} = \frac{2\pi D_{\gamma_c} (\tau_{\text{avg}})^2}{G_{\gamma_c}} \tag{2}$$

where  $D_{\gamma c}$  = damping ratio corresponding to  $\gamma_c$ , again determined from the MRD curves. The value of  $\tau_{\rm avg}$  can be estimated in the same way as in the simplified stress-based liquefaction models (Seed and Idriss 1971)

$$\tau_{\text{avg}} = 0.65 \cdot \frac{a_{\text{max}}}{g} \cdot \sigma_v \cdot r_d \tag{3}$$

where g = acceleration due to gravity in the same units as  $a_{\rm max}$ ;  $\sigma_v$  = total vertical stress at the depth of interest in the same units as  $\tau_{\rm avg}$ ; and  $r_d$  = dimensionless stress reduction factor that accounts for the nonrigid response of the soil profile.  $G_{\gamma c}$  can be estimated as  $G_{\rm max} \cdot (G/G_{\rm max})_{\gamma c}$ , where G is the secant shear modulus corresponding to  $\gamma_c$  (i.e.,  $G_{\gamma c}$ ), and  $G_{\rm max}$  is the small-strain shear modulus of the soil. The values of  $D_{\gamma c}$  and  $(G/G_{\rm max})_{\gamma c}$  can be estimated iteratively using MRD curves (e.g., Ishibashi and Zhang 1993; Darendeli 2001), where  $\gamma_c$  can be estimated as follows (e.g., Dobry et al. 1982):

$$\gamma_c = 0.65 \frac{\frac{a_{\text{max}}}{g} \cdot \sigma_v \cdot r_d}{G_{\text{max}}(G/G_{\text{max}})_{\gamma_c}} \tag{4}$$

Finally, dissipated energy per unit volume of soil for the entire duration of shaking can be estimated as  $\Delta W_{1,eq}$  multiplied by the number of equivalent loading cycles  $(n_{eq,M})$  for an earthquake of magnitude M:

$$\Delta W = \Delta W_{1,eq} \cdot n_{eq,M} = \frac{2\pi D_{\gamma c} \left[0.65 \cdot \frac{a_{\max}}{g} \cdot \sigma_v \cdot r_d\right]^2}{G_{\max} \cdot \left(\frac{G}{G_{\max}}\right)_{\gamma c}} \cdot n_{eq,M} \quad (5)$$

where  $n_{eq,M}$  can be estimated for earthquake ground motions using established correlations with M,  $a_{\rm max}$ , tectonic setting, and so on (e.g., Lasley et al. 2017). In this regard, the  $n_{eq,M}$  relationship proposed by Lasley et al. (2017) is specifically recommended over

other proposed relationships because it is derived using dissipated energy concepts. The equation for the Lasley et al. (2017)  $n_{eq,M}$  relationship is detailed subsequently in this paper.

Also, the relationship between  $\Delta W$  and the more traditionally used liquefaction triggering IM, CSR\*, is discussed in the "Discussion" section of this paper. However, it is emphasized that  $\Delta W$  is not a just a scaled variant of CSR\*. The reason for this is because the damping and shear modulus factors in Eq. (5) [i.e.,  $D_{\gamma c}$  and  $G_{\max}(G/G_{\max})_{\gamma c}$ ] are not constants, but vary as a function of the induced shear strain,  $\gamma_c$ , which in turn will be a function of the imposed shear stress, stiffness of the soil, shear stress—shear strain response of the soil, and so on. As a result,  $\Delta W$  inherently takes into account certain aspects of the influence of initial effective confining stress and aging effects on liquefaction triggering, which need to be accounted for by additional relationships when CSR is used as the IM.

#### **Case History Database**

In the absence of a liquefaction case history database that contains  $\Delta W$  information determined using a more rigorous approach, the simplified equation for estimating  $\Delta W$  [i.e., Eq. (5)] is used in conjunction the Boulanger and Idriss (2014) (BI14]) liquefaction case history database to develop an energy-based triggering model. This database was originally compiled and used to derive the Boulanger and Idriss (2016) simplified stress-based triggering model. Liquefaction case history databases have evolved over time, particularly following each significant earthquake in which liquefaction was observed. In recent years, a collaborative effort by the next generation liquefaction (NGL) project has led to the development of an open database of liquefaction case histories (Brandenberg et al. 2020; Zimmaro et al. 2019). At the time that the study herein was performed, the NGL database was not yet fully populated with case histories nor vetted by the community. In addition, the objective data included in the NGL database do not provide recommendations for critical layer selections (i.e., the layer most likely to liquefy in a given profile). Accordingly, the authors have chosen to use the BI14 liquefaction case history database in this study.

The BI14 database contains 253 case histories with estimates of earthquake parameters (e.g.,  $a_{\text{max}}$  and M), soil parameters associated with the critical layer (e.g., CPT metrics,  $\sigma_v$ , initial vertical effective stress  $\sigma'_{vo}$ , and depth to the center of the critical layer z), and observations of liquefaction response (Yes, No, or Marginal). Traditionally, these labels have been interpreted as Yes indicating that liquefaction having been triggered, No as indicating liquefaction not having been triggered, and Marginal as a case that falls somewhere in between the Yes and No cases, although the criteria used to distinguish Marginal cases from Yes or No cases are ambiguous across various studies (NRC 2016). Setting the ambiguity in the definition of Marginal cases aside for now, Upadhyaya et al. (2022) rightfully contended that the Yes and No cases can be more accurately interpreted as cases in which surficial liquefaction manifestations (e.g., sand boils and lateral spread displacements) were and were not observed following an earthquake. This alternative interpretation of the case history categories is important in evaluating the efficacy of proposed liquefaction triggering models, as discussed subsequently.

As detailed in the Supplemental Materials, for some of the case histories compiled in BI14, we revised the interpretation of parameters for the critical layers: depth, in situ soil stresses, fines content (FC), and  $q_{c1Ncs}$ . The values of  $a_{\rm max}$  and M were also reviewed for the compiled case histories.

# **Analysis of Case Histories**

Based on the findings of Lasley (2015) and Ulmer (2019),  $\Delta W$  is normalized by  $\sigma'_{vo}$  to account for the influence of initial effective confining stress on liquefaction. The sufficiency of this stress normalization is discussed in more detail in the "Discussion" section of this paper. The following sections outline the relationships used to compute  $\Delta W/\sigma'_{vo}$  for the case histories in the database.

# Stress Reduction Factor, rd

The dimensionless stress reduction factor,  $r_d$ , accounts for the nonrigid response of the soil profile when subjected to earthquake shaking. Because the case histories in the database were predominantly located in shallow-crustal active tectonic regimes, the values of  $r_d$  are estimated as a function of z and M using a relationship specifically developed for shallow-crustal events in active tectonic regimes [e.g., western US (WUS] as follows (Lasley et al. 2016):

$$r_d = (1 - \alpha) \exp\left(-\frac{z}{\beta}\right) + \alpha$$
 (6a)

$$\alpha = \exp(-4.373 + 0.4491 \cdot M) \tag{6b}$$

$$\beta = -20.11 + 6.247 \cdot M \tag{6c}$$

where z is measured in meters.

# Number of Equivalent Cycles, n<sub>eq,M</sub>

The value of  $n_{eq,M}$  is estimated using a relationship developed by Lasley et al. (2017). The relationship was developed using a low-cycle implementation of the Palmgren-Miner fatigue theory (Green and Terri 2005) and accounts for plastic response of the soil and for multidirectional shaking. The recommended form of the equation used in this study is

$$\ln(n_{eq,M}) = 0.4605 - 0.4082 \ln(a_{\text{max}}) + 0.2332M \tag{7}$$

where  $a_{\text{max}}$  is in g. As with the  $r_d$  correlation, the relationship for shallow-crustal active tectonic regimes proposed by Lasley et al. (2017) is used to analyze the case histories.

# Dynamic Soil Properties: $G_{\gamma c}$ and $D_{\gamma c}$

The values for  $G_{\gamma c}$  and  $D_{\gamma c}$  are solved iteratively using MRD curves. The iterative process entails assuming a value for  $(G/G_{\rm max})_{\gamma c}$  in the first iteration and a value of  $\gamma_c$  calculated using Eq. (4). In subsequent iterations, the ratio of  $(G/G_{\rm max})_{\gamma c}$  is obtained from a shear modulus reduction curve (e.g., Ishibashi and Zhang 1993; Darendeli 2001) corresponding to the  $\gamma_c$  calculated in the previous iteration. This process is repeated until the assumed  $(G/G_{\rm max})_{\gamma c}$  value converges to the MRD curve, similar to the iterative process used in equivalent linear site response analyses [e.g., SHAKE91 (Idriss and Sun 1992)].  $G_{\gamma c}$  is computed as  $G_{\rm max}(G/G_{\rm max})_{\gamma c}$ . The value of  $D_{\gamma c}$  is selected from a compatible damping curve at the same final value of  $\gamma_c$ .

In this study, the Ishibashi and Zhang (1993) (IZ93) curves are used to estimate  $(G/G_{\rm max})_{\gamma c}$  and  $D_{\gamma c}$ . The reason for this is that the functional form of the IZ93 equations captures the  $\tau-\gamma$  response of the soil across all strains of interest better than the modulus reduction curves that use a hyperbolic function as their base equation (e.g., Darendeli 2001; Menq 2003). For these latter curves, a moderate-to-large strain strength correction is often applied to better capture the  $\tau$ - $\gamma$  response of the soil for larger strains (e.g., Yee et al. 2013). Moreover, Green et al. (2022) found that the effective

stress-dependency term in the IZ93 relationship was in better accord with cyclic laboratory data than those for other MRD relationships examined.

Use of the IZ93 shear modulus reduction and damping curves require estimated values of the plasticity index (PI) and initial mean effective stress ( $\sigma'_{mo}$ ) as input variables. For some case histories, the PI of the critical layer was measured, but for other case histories where PI is unknown but assumed to be zero (i.e., nonplastic), the value of  $\sigma'_{mo}$  was computed as  $[(1+2K_o)/3]\cdot\sigma'_{vo}$ , where  $K_o$  is the at-rest lateral earth pressure coefficient. A limited parametric study showed that the choice of  $K_o$  had negligible influence on the computed values of  $\Delta W$ , and as a result, for simplicity,  $K_o$  was assumed to be 0.5 for all case histories.

#### Small-Strain Shear Modulus: Gmax

The values of  $G_{\rm max}$  were estimated for the soil in situ as  $G_{\rm max} = (\gamma_{t,\rm soil}/g) \cdot V_S^2$ , where  $\gamma_{t,\rm soil}$  is the total unit weight of the soil, g is the acceleration due to gravity, and  $V_S$  is the small-strain shearwave velocity. If  $V_S$  of the soil is not measured in situ, it can be estimated for young deposits using a correlation with standard penetration tests (SPT) or CPT data. There are many such correlations in the literature (e.g., Wair et al. 2012), but it is not certain whether these provide consistent or biased values of  $V_S$  if SPT versus CPT data were used, or vice versa. Ulmer et al. (2020) regressed a relationship such that stress-based liquefaction resistance curves based on  $V_S$ , CPT, and SPT metrics align. The relationship specific for CPT data is

$$V_S = 16.88 (q_{c1Ncs})^{0.489} \left(\frac{\sigma'_{vo}}{P_a}\right)^{0.25}$$
 (8)

where  $V_S$  is in meters per second; and  $P_a$  = atmospheric pressure in the same units as  $\sigma'_{vo}$ . For this study,  $G_{\rm max}$  was estimated using this relationship assuming  $\gamma_{t,\rm soil}$  equal to 17.0 and 19.5 kN/m³ above and below the groundwater table, respectively (e.g., Moss 2003; Green et al. 2014) for all case histories in the database (Table S1). Table 1 provides a summary of how each input parameter was obtained for this study.

#### Input Parameter Uncertainties

To develop a probabilistic limit-state curve for the proposed energy-based method, the uncertainties associated with each input parameter must be addressed, including an estimate of the uncertainty in  $q_{c1Ncs}$  and  $\Delta W/\sigma'_{vo}$ . It was assumed that  $\Delta W/\sigma'_{vo}$  was lognormally distributed with a standard deviation of  $\sigma_{\ln(\Delta W/\sigma'_{vo})}$ . The equation for  $\Delta W/\sigma'_{vo}$  required to trigger liquefaction, written as a natural log, is

$$\ln\left(\frac{\Delta W}{\sigma_{vo}'}\right) = \ln(2\pi g \cdot 0.65^{2}) + \ln(D_{\gamma_{c}}) + 2\ln(a_{\text{max}}) + 2\ln(\sigma_{v}) 
+ 2\ln(r_{d}) + \ln(n_{eq,M}) - \ln(\gamma_{t,\text{soil}}) - \ln(\sigma_{vo}') 
- 2\ln(V_{S}) - \ln\left[\left(\frac{G}{G_{\text{max}}}\right)_{\gamma}\right]$$
(9)

The value of  $\sigma_{\ln(\Delta W/\sigma'vo)}$  was estimated using a first-order, second-moment estimation method using the uncertainties of each input parameter:  $D_{\gamma c}, \ln(a_{\max}), \ \sigma_v, \ r_d, \ \ln(n_{eq,M}), \ \gamma_{t,\mathrm{soil}}, \ \sigma'_{vo}, \ln(V_S)$ , and  $(G/G_{\max})_{\gamma c}$ . The matrix notation for this first-order approximation is

$$\sigma_{\ln\left(\frac{\Delta W}{\sigma_{vo}'}\right)}^2 = \nabla^T \Sigma_{xx} \nabla \tag{10a}$$

$$\nabla = \begin{bmatrix} \frac{\partial}{\partial D_{\gamma_c}} \ln\left(\frac{\Delta W}{\sigma'_{vo}}\right) \\ \frac{\partial}{\partial \ln a_{\max}} \ln\left(\frac{\Delta W}{\sigma'_{vo}}\right) \\ \vdots \\ \frac{\partial}{\partial (G/G_{\max})_{\gamma_c}} \ln\left(\frac{\Delta W}{\sigma'_{vo}}\right) \end{bmatrix}$$
(10b)

$$\Sigma_{xx} = \begin{bmatrix} \sigma_D^2 & \rho_{D,\ln a_{\max}} \sigma_D \sigma_{\ln a_{\max}} & \cdots & \rho_{D,G/G_{\max}} \sigma_D \sigma_{G/G_{\max}} \\ \rho_{D,\ln a_{\max}} \sigma_D \sigma_{\ln a_{\max}} & \sigma_{\ln a_{\max}}^2 & \cdots & \vdots \\ \vdots & \vdots & \ddots & \vdots \\ \rho_{D,G/G_{\max}} \sigma_D \sigma_{G/G_{\max}} & \cdots & \sigma_{G/G_{\max}}^2 \end{bmatrix}$$

$$(10c)$$

where the value of  $\rho$  in each term is the correlation coefficient of the pair of variables represented in the term. All variables were assumed to be normally distributed except for  $V_S$ ,  $a_{\rm max}$ , and  $n_{eq,M}$ , which were assumed to be lognormally distributed. The value of  $\gamma_{t,\rm soil}$  was an assumed constant for all case histories, and thus its uncertainty was not considered. Table 2 summarizes the standard deviations and correlation coefficients required to estimate  $\sigma_{\ln(\Delta W/\sigma'vo)}$ , where all variables are assumed to be uncorrelated except for the pairs of variables with values of  $\rho$  included in Table 2. Justifications for each estimate of uncertainty are also provided, and uncertainties that require more detailed explanations are discussed next.

The standard deviation of  $q_{c1Ncs}$  (i.e.,  $\sigma_{qc1Ncs}$ ) was estimated using a coefficient of variation (COV) of COV =  $\sigma_{qc1Ncs}/q_{c1Ncs}$ . The adopted value of COV was determined from a set of over 3,000 CPT soundings from the Christchurch, New Zealand, region (data from Upadhyaya 2019; Geyin et al. 2021). Each sounding was divided into individual soil layers that were sufficiently thick (e.g., at least 1 m) to estimate  $\sigma_{qc1Ncs}$  within each layer.

The average COV from all of the soundings in the database was reasonably constant with depth and was approximately 0.093. When FC is estimated from  $I_c$ , instead of measured in a laboratory, the COV is increased by a factor of 1.5 (e.g., Boulanger and Idriss 2014). This estimate of COV represents variability in  $q_{c1Ncs}$  vertically within the thickness of a single soil layer detected from a CPT sounding and does not account for the uncertainties due to lateral variability or measurement error.

Estimates of the standard deviation of  $\ln(a_{\text{max}})$  [i.e.,  $\sigma_{\ln(a_{\text{max}})}$ ] were extracted directly from USGS ShakeMaps (USGS 2019) when geographic coordinates were able to be determined for the case history sites. Some exceptions include the following:

- When geographic coordinates were not able to be determined, the mean value of  $\sigma_{\ln(a_{\max})}$  within the map extents of each earthquake was adopted.
- In the case of the 1964 Niigata, Japan, event, no ShakeMap is available. Instead, σ<sub>In(a<sub>max</sub>)</sub> was estimated based on an estimate of the standard deviation of a<sub>max</sub> (i.e., σ<sub>a<sub>max</sub></sub>) given by Moss et al. (2006) for this specific event. Their assumption was that

**Table 1.** Required parameters to compute  $\ln(\Delta W/\sigma'_{vo})$ 

Parameter	Equation	Notes
$\sigma_v$	$\gamma_A \cdot (z_w) + \gamma_{t, \text{soil}} \cdot (z - z_w)$	$z_w$ = depth to groundwater table (gwt) and $\gamma_A = 17.0 \text{ kN/m}^3$
$\sigma'_{vo}$	$\sigma_v - \gamma_w(z - z_w)$	$\gamma_w = 9.81 \text{ kN/m}^3$
$ln(V_s)$	Eq. (8)	Ulmer et al. (2020)
$\gamma_{t,\mathrm{soil}}$	19.5 kN/m <sup>3</sup> below gwt ( $z > z_w$ ) 17.0 kN/m <sup>3</sup> above gwt( $z \le z_w$ )	Assumed value below the groundwater table (Moss 2003; Green et al. 2014)
$(G/G_{ m max})_{\gamma c}$	Iterative computation: Eq. (4)	Assume $K_o = 0.5$ to compute $\sigma'_{mo}$ and assume PI = 0, unless given
$D_{\gamma c}$	Compatible with $(G/G_{ m max})_{\gamma c}$	Assume $K_o = 0.5$ to compute $\sigma'_{mo}$ and assume PI = 0, unless given
$r_d$	Eq. (6)	Lasley et al. (2016) (WUS-specific)
$\ln(n_{eq,M})$	Eq. (7)	Lasley et al. (2017) (WUS-specific)
$\ln(\frac{a_{\max}}{g})$	Varies for each case history	From strong motion recordings, USGS ShakeMaps, or regional ground motion models. Converted from peak to geometric mean $a_{\text{max}}$ values when necessary

**Table 2.** Standard deviations and correlation coefficients required to compute  $\sigma_{\ln(\Delta W/\sigma'_{re})}$ 

Parameter	Equation	Notes	
$\sigma_{q_{c1Ncs}}$	$0.093 \cdot q_{c1Ncs}$ FC measured in the lab $0.1395 \cdot q_{c1Ncs}$ FC estimated from $I_c$	From analysis of CPTs in Christchurch, New Zealand	
$\sigma_{\sigma_v}$ $\sigma_{\sigma'_{vo}}$	$\sqrt{0.56 + 380.25 \left(\frac{T}{6}\right)^2}$ (kPa) $\sqrt{4.8 + 93.89 \left(\frac{T}{6}\right)^2}$ (kPa)	T = thickness of critical layer (m). From assumed uncertainties in depth to critical layer and depth to groundwater table	
$\sigma_{V_s}$	$\sigma_{\ln V_s} = \left(rac{0.489}{q_{c1Ncs}} ight)\!\sigma_{q_{c1Ncs}}^2 + \left(rac{0.25}{\sigma_{vo}'} ight)\!\sigma_{\sigma_{vo}'}^2$	First-order approximation	
$\sigma_{G/G_{ m max}}$	Varies (function of shear strain)	Darendeli (2001)	
$\sigma_D$	Varies (function of shear strain)	Darendeli (2001)	
$\sigma_{r_d}$	$\frac{0.1506}{1 + \exp(-0.4975z)}$	Lasley et al. (2016) (WUS-specific)	
$\sigma_{\ln(n_{eq})}$	$\max \left\{ \begin{array}{c} 0.5399 - (2.928 \times 10^{-3})z \\ 0.4626 \end{array} \right\}$	Lasley et al. (2017) (WUS-specific)	
$\sigma_{\ln(a_{ ext{max}})}$	Varies	In general: from USGS ShakeMaps and increased to account for uncertainty in conversion from peak to geometric mean $a_{\rm max}$	
$ ho_{D,G/G_{ ext{max}}}$	-0.5	Rodriguez-Marek et al. (2014)	
$ ho_{\sigma'_{vo},\sigma_v}$	-1.0	Based on uncertainty in groundwater table	
$\rho_{r_d,\ln(n_{eq})}$	$-0.0390(z) - 0.1251$ for $z \le 8.7$ m $-0.4644$ for $z > 8.7$ m	Based on analyses of site-response analyses performed by Lasley et al. (2016, 2017)	
$\rho_{\ln(a_{\max}),r_d}$	-0.0062(z) - 0.1692	Based on analyses of site-response analyses performed by Lasley et al. (2016, 2017)	
$ \rho_{\ln(a_{\max}),\ln(n_{eq})} $	$0.0310(z) - 0.3710$ for $z \le 12.5$ m $0.0165$ for $z > 12.5$ m	Based on analyses of site-response analyses performed by Lasley et al. (2016, 2017)	

 $a_{\rm max}=0.162g\pm0.03g$ . Assuming that the  $\pm0.03g$  represents one standard deviation of  $a_{\rm max}$  (i.e.,  $\sigma_{a_{\rm max}}$ ), the corresponding  $\sigma_{\ln(a_{\rm max})}$  was computed as follows:

$$\sigma_{\ln(a_{\max})} = \sqrt{\ln\left[1 + \left(\frac{\sigma_{a_{\max}}}{a_{\max}}\right)^{2}\right]} = \sqrt{\ln\left[1 + \left(\frac{0.03}{0.162}\right)^{2}\right]}$$

$$= 0.1836 \tag{11}$$

• Estimates of  $\sigma_{\ln(a_{\max})}$  for the 2010 M7.1 Darfield and 2011 M6.2 Christchurch events were obtained directly from the Bradley (2013) model to be consistent with the estimates of  $a_{\max}$  from the same model.

If the value of  $a_{\rm max}$  for a given case history was converted from a peak value to a geometric mean  $a_{\rm max}$  as discussed previously, then its standard deviation was also increased to reflect the uncertainty in the conversion

$$\sigma_{\ln GMa_{\text{max}}}^2 = \sigma_{\ln \text{Peak}a_{\text{max}}}^2 + \sigma_{\ln(\text{Peak}/GM)}^2 \tag{12}$$

where  $\sigma_{\ln GMa_{\max}}$  = standard deviation of the converted geometric mean  $a_{\max}$ ;  $\sigma_{\ln Peak_{a_{\max}}}$  = original estimate of  $\sigma_{\ln a_{\max}}$  associated with the peak value  $a_{\max}$ ; and  $\sigma_{\ln (Peak/GM)}$  = uncertainty in the conversion: 0.091 (Boore and Kishida 2017).

Ishibashi and Zhang (1993) did not provide standard deviations for their values of  $D_{\gamma c}$  and  $(G/G_{\rm max})_{\gamma c}$ . However, it was assumed that the standard deviations of  $D_{\gamma c}$  and  $(G/G_{\rm max})_{\gamma c}$  estimated by

Darendeli (2001) as a function of strain is reasonably applicable for the IZ93 values as well.

#### Regression of the Limit-State Function

A limit-state surface separating the Yes liquefaction from the No liquefaction case histories is developed using maximum likelihood regression. The limit-state function can be denoted

$$g = f(q_{c1Ncs}, \Theta) - \ln\left(\frac{\Delta W}{\sigma'_{no}}\right) + \varepsilon \tag{13}$$

where f = function of a chosen form (e.g., linear or power);  $\Theta$  is a vector of coefficients; and  $\varepsilon$  = error term that is assumed to be normally distributed with a mean of zero and standard deviation of  $\sigma_{\varepsilon}$ . The limit state is obtained by setting g=0: if  $g\leq 0$ , liquefaction is predicted and if g>0, liquefaction is not predicted. The liquefaction case history database provides the vector of variables that define the dissipated energy [i.e.,  $D_{\gamma c}$ ,  $(G/G_{\max})_{\gamma c}$ ,  $G_{\max}$ ,  $V_S$ ,  $a_{\max}$ ,  $r_d$ ,  $\sigma'_{vo}$ ,  $\sigma_v$ , and  $n_{eq,M}$ ] and the resistance,  $q_{c1Ncs}$ , where the vector of variables for a given case history is denoted by  $X_i$ . The parameters of the limit-state surface ( $\Theta$ ), which include the uncertainty parameter  $\sigma_{\varepsilon}$ , are obtained through regression. The likelihood function can then be computed (Cetin et al. 2002)

$$L(\Theta, \sigma_{\varepsilon}) = \prod_{\text{Liq. sites}} P[g(X_i, \Theta) \le 0] \times \prod_{\text{No-liq. sites}} P[g(X_i, \Theta) > 0]$$

$$\tag{14}$$

where the first term quantifies the probability of g being less than or equal to zero at liquefied sites and the second term quantifies the probability of g being greater than zero at nonliquefied sites. The values of the  $\Theta$  vector, including the standard deviation  $\sigma_{\varepsilon}$ , are then regressed to maximize the likelihood, L. Alternatively, the log-likelihood function can be maximized using this equation:

$$\begin{split} \ln(L(\Theta,\sigma_{\varepsilon})) &= \sum_{\text{Liq. sites}} \ln(P[g(X_i,\Theta) \leq 0]) \\ &+ \sum_{\text{No-liq. sites}} \ln(P[g(X_i,\Theta) > 0]) \end{split} \tag{15}$$

If uncertainties in the input parameters are not considered, then the probability of liquefaction,  $P_L$ , can be written

$$P_L = P[g(X_i, \Theta) \le 0] = 1 - \Phi\left[\frac{g(X_i, \Theta)}{\sigma_{\varepsilon}}\right]$$
 (16)

where  $\Phi(\cdot)$  = standard normal cumulative distribution function. If the uncertainties in the input parameters are considered, then each input parameter has its own mean and error term. Thus, the probability of liquefaction is estimated

$$\begin{split} P_L &= P[g(X_i, \Theta) \leq 0] \\ &= \iint \left( 1 - \Phi\left[\frac{g(X_i, \Theta)}{\sigma_{\varepsilon}}\right] \right) f_{\mathcal{Q}}(q) f_W(\omega) dq d\omega \end{split} \tag{17}$$

where  $\omega = \ln(\Delta W/\sigma'_{vo})$ ;  $q = q_{c1Ncs}$ ; and  $f_Q(q)$  and  $f_W(\omega) =$  probability density functions of  $q_{c1Ncs}$  and  $\ln(\Delta W/\sigma'_{vo})$ , respectively. As indicated previously,  $f_W$  was assumed to be lognormally distributed with an uncertainty estimated using Eq. (10). Similarly,  $f_Q$  was assumed to be normally distributed with the standard deviation given in Table 2.

As noted by Boulanger and Idriss (2014), outliers with very low probabilities of  $P[g(X_i,\Theta,\varepsilon_i)\leq 0]$  or  $P[g(X_i,\Theta,\varepsilon_i)>0]$  can have a strong influence on the outcome of the regression. Thus, for practicality, it is reasonable to set a minimum probability for any one case history,  $P_{\min}$  (effectively stating that any site on the liquefaction side of the limit-state surface has a minimum probability of noliquefaction of  $P_{\min}$ , and conversely any site on the no-liquefaction side of the limit-state surface has a minimum probability of liquefaction of  $P_{\min}$ ). Boulanger and Idriss used a sensitivity analysis to test the effect of a range of  $P_{\min}$  values on their regression and found  $P_{\min}$  values between 0.05 and 0.075 to be realistic. In the present study, a range of  $P_{\min}$  values was also considered, and  $P_{\min}=0.05$  was selected based on the stabilizing effect it had on the regression while not altering the regression coefficients significantly compared with lower values of  $P_{\min}$ .

The limit-state curve was regressed two ways, first assuming that the input parameters are known (i.e., input parameter uncertainties are not considered) and then assuming that the input parameters have some uncertainty (e.g., Cetin et al. 2002). Several functional forms were considered for the regression. However, balancing the desires to limit the complexity of the functional form and having a shape that yielded the best predictive rates for the case histories in our database, a power fit was chosen for the limit-state curve as follows:

$$\ln\left(\frac{\Delta W}{\sigma'_{vo}}\right)_{\text{liq}} = c_1(q_{c1Ncs})^{c_2} - 7.52 + \varepsilon \tag{18}$$

The intercept was fixed to a value of -7.52 to stabilize the regression because the data are not sufficient to constrain  $c_1$ ,  $c_2$ ,  $\sigma_{\varepsilon}$ , and the intercept term. The value of -7.52 matches the intercept from a laboratory-derived liquefaction resistance curve (Ulmer 2019), which was assumed to be closely associated with a lower bound of the general field-based limit-state curve. Table 3 contains the regression coefficients for the limit-state curve for two scenarios: excluding and including the uncertainties in the input parameters.

The uncertainty in the limit-state curve,  $\sigma_{\varepsilon}$ , was smaller when the uncertainties in the input parameters were included [Eq. (17)]. This represents a case in which  $\sigma_{\varepsilon}$  is an estimate of true model error; the larger resulting uncertainty when ignoring uncertainties in the input parameters [Eq. (16)] can be thought of as total uncertainty (e.g., Franke and Olson 2021). Fig. 2 shows how these limit-state curves fit the data from the case history database. A deterministic triggering curve is also shown in Fig. 2 and is discussed subsequently. One case history with  $q_{c1Ncs}$  of nearly 300 was treated as an outlier and ignored in the regression so that it would not have undue influence on the resulting limit-state curve

At first glance, the number of No liquefaction cases above the curves and the number of Yes liquefaction cases below the curves seem unusually high. These issues can be explained, at least partially, by additional considerations as discussed subsequently in the "Discussion" section of this paper. Figs. S1–S4 show the same case histories split up into various intervals of FC,  $\sigma'_{vo}$ , M, and  $a_{\rm max}$  values, respectively. These figures illustrate the model performance for different ranges of applicability of the predictive variables.

**Table 3.** Regression coefficients for energy-based limit-state curves for two scenarios: uncertainties in input parameters excluded and uncertainties included

Scenario	$c_1$	$c_2$	$\sigma_{arepsilon}$
Uncertainties excluded [Eq. (16)]	$1.224 \times 10^{-7}$	3.352	1.590 (total)
Uncertainties included [Eq. (17)]	$1.223 \times 10^{-7}$	3.335	1.400 (model)

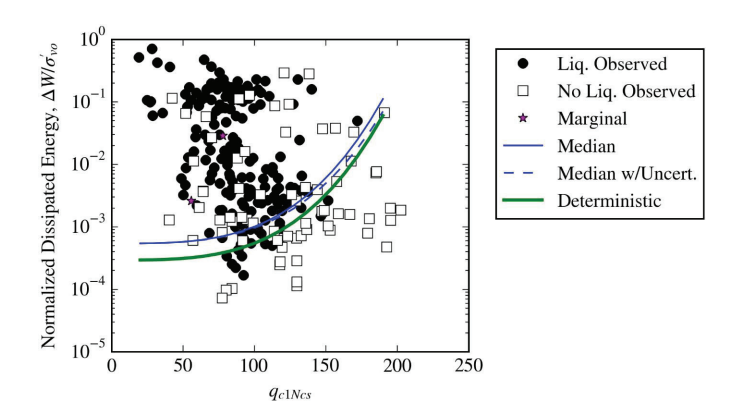


**Fig. 2.** Case histories from the updated database plotted as normalized dissipated energy versus  $q_{c1Ncs}$ . Also shown are median ( $P_L = 50\%$ ) energy-based limit-state curves for two scenarios: uncertainties in input parameters are ignored and uncertainties are included. Bold line represents deterministic curve.

## Implementation in Forward Analysis

To implement the proposed energy-based triggering model for predicting the occurrence of liquefaction, the following equation can be used to compute  $P_L$  for a given layer of soil (assuming no uncertainty in the input parameters, i.e., using total uncertainty for the limit-state curve and best-estimated values for each input parameter):

$$P_L = 1 - \Phi \left[ \frac{(1.224 \times 10^{-7})(q_{c1Ncs})^{3.352} - 7.52 - \ln(\frac{\Delta W}{\sigma'_{ro}})}{1.590} \right]$$
(19)

where  $\ln(\Delta W/\sigma'_{vo})$  can be computed using Eq. (5) or via more refined methods (e.g., equivalent linear numerical site response analyses using the IZ93 MRD curves and several input motions representative of the design event).

The recommended deterministic estimate of  $\ln(\Delta W/\sigma'_{vo})$  to trigger liquefaction [i.e.,  $\ln(\Delta W/\sigma'_{vo})_{\rm liq}$ ] is

$$\ln\left(\frac{\Delta W}{\sigma'_{vo}}\right)_{\text{liq}} = 1.224 \times 10^{-7} \cdot (q_{c1Ncs})^{3.352} - 8.133 \tag{20}$$

which is associated with a  $P_L = 35\%$  contour computed using the total uncertainty. The factor of safety against liquefaction triggering, FS<sub>L</sub>, is then computed

$$FS_L = \frac{\ln\left(\frac{\Delta W}{\sigma_{vo}^{\prime}}\right)_{\text{liq}}}{\ln\left(\frac{\Delta W}{\sigma^{\prime}}\right)} \tag{21}$$

where  $\ln(\Delta W/\sigma'_{vo})$  and  $\ln(\Delta W/\sigma'_{vo})_{liq}$  can be computed using Eqs. (5) and (20), respectively, or by more refined methods. The  $P_L=35\%$  contour was chosen as the deterministic curve because it reasonably aligned the distribution of FS<sub>L</sub> from Eq. (21) with the distribution of FS<sub>L</sub> from stress-based methods (e.g., Boulanger and Idriss 2014; Green et al. 2019) and is consistent with the total uncertainty  $P_L$  used by Green et al. (2019) in defining their deterministic triggering curve. Although a deterministic estimate of FS<sub>L</sub> is frequently the goal of liquefaction evaluations in current practice, the use of a full probabilistic approach allows the user to adopt a probability of liquefaction that is consistent with a desired or target risk level.

#### **Discussion**

As mentioned in the "Introduction" and "Background" sections, there are several characteristics that are desired in liquefaction triggering models. Some of these characteristics relate to the IM used to parameterize the demand. For any alternative IM used in engineering analyses, the lack of maturity in models for predicting the IM is a concern (e.g., Is the benefit in refining the liquefaction triggering prediction using a "new and improved" IM offset by the increased uncertainty in predicting the IM?). Additionally, the IM should relate mechanistically to excess pore-water pressure generation and should be consistent with seismic hazard maps issued by building regulators. In the simplified form proposed in this paper the predictive variables for  $\Delta W$  are similar to those used to compute CSR\* in the stress-based approaches, hence there is no additional uncertainties introduced in the prediction of the IM.

Two other requirements for an IM are sufficiency and efficiency (Luco and Cornell 2007). Efficiency is evaluated by the predictive ability of the model, which is discussed subsequently in this section. We postulate that sufficiency is addressed by ensuring that the

IM relates physically to the process that is being predicted (i.e., pore pressure generation and liquefaction triggering). As discussed previously,  $\Delta W$  relates mechanistically to excess pore-water pressure generation (e.g., Nemat-Nasser and Shokooh 1979; Simcock et al. 1983; Berrill and Davis 1985; Figueroa et al. 1994; Green et al. 2000; Davis and Berrill 2001; Jafarian et al. 2012; Polito et al. 2008; Kokusho and Kaneko 2018; Kokusho and Tanimoto 2021; among many others).

Another desired characteristic of liquefaction triggering models is that these models should allow for correlations between the ability of the soil to resist liquefaction and in situ test metrics, circumventing issues about the representativeness of laboratory specimen versus in situ soil response (e.g., Peck 1979). Two additional desired model characteristics relate to implementation scalability of the model (i.e., the model should allow refined estimates of either earthquake loading or ability of the soil to resist liquefaction to be readily incorporated) and to the applicability of the triggering curve for non-reference conditions (e.g., non-vertically-propagating wave fields or nonearthquake loading). These two attributes are further discussed subsequently as related to the proposed model. Also, as elaborated subsequently, an attribute that relates to the overall validity of the model, in addition to being a desired characteristic, is that a model should consistently operate within either a total stress or effective stress framework. With all of this in mind, the authors' proposed energy-based liquefaction triggering model is not burdened by these issues.

# Choice of AW as an Energy IM

As mentioned in the "Background" section of this paper, various IMs for liquefaction triggering evaluation models have been broadly classified as energy-based procedures, to include  $I_A$  and CAV. The justification for using these IMs is commonly based on numerical effective stress site response analyses were  $I_A$  or CAV of the input motion is correlated to the computed excess pore-water response somewhere in the soil profile (e.g., Kramer and Mitchell 2006; Bullock et al. 2022). To estimate the  $I_A$  associated with liquefaction triggering in cyclic laboratory tests, Green (2001) derived the following expression for soil samples subjected to cyclic simple shear, wherein the loading is sinusoidal, acting in one direction, and has a constant frequency and amplitude shear stress:

$$I_A = \frac{n\pi g \, \tau^2}{4\sigma_n^2} \tag{22}$$

where  $\sigma_v$  = total vertical stress; g = acceleration due to gravity; n = number of cycles of loading; and f and  $\tau$  frequency and amplitude of the applied shear stress. When n equals the number of cycles required to initiate liquefaction in the sample,  $I_A$  computed using Eq. (22) equals the capacity of the soil  $(I_{A,\text{liq}})$ .

Eq. (22) is revealing in two ways. First,  $I_{A,\mathrm{liq}}$  is independent of effective confining stress, and second,  $I_{A,\mathrm{liq}}$  is a function of the frequency of loading; numerous laboratory studies have shown trends contradicting both of these (e.g., Lee and Seed 1967; Seed 1983; Riemer et al. 1994). Focusing on the frequency dependency issue, Riemer et al. (1994) performed undrained stress-controlled cyclic triaxial tests on Monterey 0 sand, where the applied sinusoidal loading ranged in frequency from 0.1 to 20 Hz. One of the conclusions from their study is that the "effect of frequency on the number of cycles to liquefaction at a given cyclic stress ratio was not significant in the stress controlled loading." Ignoring the difference in the stress paths associated with cyclic triaxial versus cyclic simple shear testing, Eq. (22) implies that the  $I_{A,\mathrm{liq}}$  for the tests loaded at 0.1 Hz would be 200 times greater than those for the tests performed at 20 Hz. In contrast, the  $(\Delta W/\sigma'_{vo})_{\mathrm{liq}}$  for these

tests have been shown to be approximately the same (e.g., Lasley 2015).

The frequency dependency of  $I_A$  triggering models is an artifact of  $I_A$  being computed by integrating the amplitude of the loading over time; this same phenomenon is an issue any IM that integrates the amplitude of loading over time (e.g., CAV). Inherently, the liquefaction triggering models that use  $I_A$  or CAV and justify the use of the IMs based on numerical effective stress site response analyses conflate profile response characteristics, which are frequency-dependent, and soil element liquefaction response characteristics, which are frequency-independent. The conflagration of distinct phenomena will ultimately limit improvements in the prediction efficacy of the models and limits the implementation scalability of the models. In contrast, these limits are not inherent to  $\Delta W$ -based models.

#### Implementation Scalability

Specific to the proposed energy-based model implemented in its simplified form, the IMs required to compute  $\Delta W/\sigma'_{vo}$  are the same as those required for simplified stress-based models (i.e.,  $a_{\rm max}$  and M), with these IMs used in conjunction with MRD curves (i.e., Ishibashi and Zhang 1993). However, refinements can be made to the loading imposed on the soil (i.e.,  $\Delta W/\sigma'_{vo}$ ). Toward this end, the refinements can be made by directly measuring  $V_S$  in situ, developing site- or region-specific  $r_d$  and/or  $n_{eq,M}$  relationships for use in Eq. (5), and/or developing soil-specific MRD curves used to compute  $\gamma_c$  [Eq. (4)]. However, the same general approaches used to derive the relationships used to develop the triggering model also should be used to develop new relationships (e.g., use of equivalent linear site response analyses using the IZ93 MRD curves) to avoid the introduction of new biases due to computational artifacts, and so on.

Additionally, if required inputs are available, equivalent linear site response analyses can be performed to estimate  $\Delta W$  directly. Toward this end, both the shear stress and shear strain time histories at the depth of interest should be output from site response analyses, and  $\Delta W$  is calculated as the cumulative area enclosed by the stress-strain hysteresis loops (Green and Terri 2005). This area can be estimated using the trapezoidal rule

$$\Delta W = \frac{1}{2} \sum_{k=1}^{n-1} (\tau_{k+1} + \tau_k) (\gamma_{k+1} - \gamma_k)$$
 (23)

where  $\tau_k$  and  $\gamma_k$  (in decimal form) = kth increments of shear stress and shear strain, respectively; and n = total number of digitized points in a time history.

Alternatively, the equivalent linear site response software Shake VT2 (Lasley 2015; Thum et al. 2019) has an option to output  $\Delta W$  directly. However, because the value for  $(\Delta W/\sigma'_{vo})_{lig}$  given by

Eq. (20) is based on the analysis of case histories where  $\Delta W/\sigma'_{vo}$  imposed on the soil was due to both components of horizontal motion during a seismic event, site response analyses need to be performed using both orthogonal components of horizontal input motions and the  $\Delta W$  for each summed together. Alternatively, the  $(\Delta W/\sigma'_{vo})_{\text{liq}}$  computed using Eq. (20) can be adjusted to allow a comparison with  $\Delta W$  computed from a single site response analysis (i.e., one input motion). In this latter approach,  $(\Delta W/\sigma'_{vo})_{\text{liq}}$  computed using Eq. (20) should be multiplied by the ratio of  $\Delta W$  for one dimension (1D) versus two dimensions (2D) given by

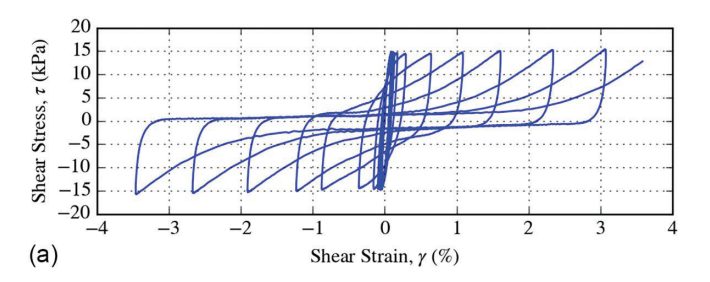
$$\ln\left(\frac{\Delta W_{\rm 1D}}{\Delta W_{\rm 2D}}\right)_{\rm liq} = -0.8248 - 0.0023 \ln(a_{\rm max}) + 0.0221 M \quad (24)$$

This relationship is based on the  $n_{eq,M}$  relationships proposed by Lasley et al. (2017) for 1D and 2D loadings.

Although, in theory, similar refinements can be made to the CSR\* for the stress-based triggering models, it would be inappropriate to compare the resulting CSR\* with the stress-based limit-state curves that use a biased  $r_d$  relationship (e.g., Green et al. 2019). Furthermore, although some stress-based models (e.g., Cetin et al. 2018; Moss et al. 2006; Kayen et al. 2013) use a  $r_d$  relationship that is not biased, these models are still dependent on a generic MSF to account for durational effects. In contrast, computation of  $\Delta W$  via site response analyses can be used to compute  $\ln(\Delta W/\sigma'_{vo})$  and compared with  $\ln(\Delta W/\sigma'_{vo})_{liq}$ , where the computed  $\Delta W$  accounts for both the amplitude and duration of shaking in a single parameter that has a physical link to liquefaction triggering (e.g., Ostadan et al. 1998).

Regarding refinements in estimating the ability of the in situ soil to resist liquefaction triggering, cyclic laboratory tests can be performed on undisturbed samples. However, as may be surmised, applying Eq. (23) directly to compute  $\Delta W$  from shear stress and shear strain time histories from undrained stress-controlled cyclic laboratory test data does not result in a value that is directly comparable to  $\Delta W$  computed using Eq. (5) or from equivalent linear site response analyses. This is because the  $\gamma$  time history obtained from undrained stress-controlled laboratory tests inherently includes the effects of the degradation of soil stiffness (i.e., G) due to excess pore-water pressure generation, whereas use of Eq. (4) to estimate  $\gamma_c$  does not (i.e., effective stress versus total stress frameworks). The inconsistent operation within a total versus effective stress framework is an inherent limitation of several previously proposed energy-based triggering models.

Fig. 3 shows an example set of hysteresis loops from a constant-volume cyclic simple shear test performed on Monterey 0/30 sand and the associated relationship between normalized dissipated energy within an effective stress framework ( $\Delta W_{\rm eff}/\sigma'_{vo}$ ) and the number of cycles of loading (N). Initially, the hysteresis loops are approximately the same size, and the relationship between



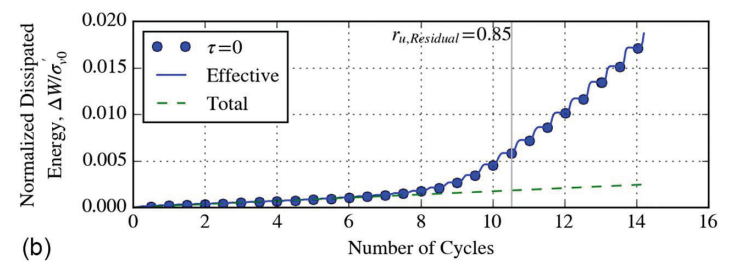


Fig. 3. Results from a cyclic direct simple shear test: (a) sample hysteresis loops; and (b) relationship between both effective and total normalized dissipated energy and number of loading cycles.

 $\Delta W_{\rm eff}/\sigma'_{vo}$  and N is linear. Once the excess pore-water pressure ratio  $(r_u)$  is sufficiently large to soften the soil, the hysteresis loops grow larger with each cycle of loading. At this point, the relationship between  $\Delta W_{\rm eff}/\sigma'_{vo}$  and N is no longer linear and tends toward an exponentially increasing shape.

The initial linear portion of the  $\Delta W_{\rm eff}/\sigma'_{vo}$  versus N plot is equivalent to a  $\Delta W/\sigma'_{vo}$  versus N computed within a total stress framework (i.e.,  $\Delta W_{\rm tot}/\sigma'_{vo}$  versus N). This is because the constant slope of the early portion of  $\Delta W_{\rm eff}/\sigma'_{vo}$  versus N plot implies that the stiffness of the soil is not significantly influenced by the excess pore-water pressure and that size of hysteresis loops is relatively constant from one cycle to the next. Accordingly, if this linear portion of the  $\Delta W_{\rm eff}/\sigma'_{vo}$  versus N curve is extrapolated, it is a reasonable representation of the  $\Delta W_{\rm tot}/\sigma'_{vo}$  versus N curve; Fig. 3(b) illustrates this relationship. Once the relationship between  $\Delta W_{\rm tot}/\sigma'_{vo}$  versus N is established, a liquefaction triggering criterion for interpreting cyclic laboratory tests (e.g.,  $r_u$ 0.85, single axial strain  $\varepsilon_{sa}$  equal to 3.5%, double axial strain  $\varepsilon_{da}$ equal to 5%, and so on) is used to determine N corresponding to liquefaction (i.e.,  $N_{\rm liq}$ ). The value of  $(\Delta W/\sigma'_{vo})_{\rm liq}$  is equal to the value of  $\Delta W_{\rm tot}/\sigma'_{vo}$  corresponding to  $N=N_{\rm liq}$ . Guiding rules for extrapolating the initial portion of the  $\Delta W_{\rm eff}/\sigma'_{vo}$  versus N curve to estimate  $\Delta W_{\rm tot}/\sigma'_{vo}$  are provided in the Supplemental Materials. Not being able to refine the estimated energy required to trigger liquefaction via undrained cyclic laboratory tests performed on undisturbed samples is an inherent limitation of several previously proposed energy-based triggering models, particularly for triggering models that use  $I_A$  or CAV as an IM, as discussed

## Applicability of Triggering Curve

One advantage of the proposed triggering curve is that its applicability is wide ranging. Within the realm of earthquake analyses, the model can be used to analyze liquefaction triggering for free-field sites, similar to simplified stress-based models, to include liquefaction triggering of aged soils using directly measured values of  $V_S$  to compute  $G_{\rm max}$  (e.g., Green et al. 2022). Furthermore, the model can be used to analyze flow liquefaction of earthen dams, for example, resulting from earthquake shaking using an approach analogous to that outlined by Naesgaard and Byrne (2007) and Beaty and Byrne (2008). In these types of analyses, the dynamic response of the dam is numerically modeled within a total stress framework and the normalized dissipated energy is tracked for each

element for each time step. Once the normalized dissipated energy exceeds that required to trigger liquefaction, the properties of the soil of that element are switched to those corresponding to the residual values of liquefied soil. Use of dissipated energy as the cumulative damage metric in these analyses is more direct than applying stress-based cycle counting methods (e.g., Naesgaard and Byrne 2007; Beaty and Byrne 2008). However, in using Eq. (20) to estimate the normalized dissipated energy required to trigger liquefaction for 1D shaking in a 2D numerical analysis, adjustments for 1D versus 2D shaking need to be applied per Eq. (24).

Outside the realm of earthquake analyses, the proposed triggering curve can be used to evaluate liquefaction due to construction vibrations [e.g., pile driving (Taylor 2011; Lamens and Askarinejad 2021)], geophysical explorations (e.g., Hryciw et al. 1990), and soil improvement (e.g., Green and Mitchell 2004, 2010), among other applications. However, for these applications, approaches for computing  $\Delta W$  associated with the vibratory loading may need to be developed. Nevertheless, not linking the duration of the ground vibrations to earthquake magnitude broadens the applicability of the triggering curve to nonearthquake-type applications.

#### Comparison of Proposed Energy-Based and Stress-Based Triggering Model Frameworks

#### Relationship between $\Delta W/\sigma'_{vo}$ and CSR\*

As detailed previously, for typical liquefaction evaluations,  $\Delta W/\sigma'_{vo}$  can be computed using Eq. (5), which inherently estimates the value of  $\tau_{\rm avg}$  via Newton's Second Law, the same as the simplified stress-based liquefaction models (Seed and Idriss 1971). However, this does not mean that  $\Delta W/\sigma'_{vo}$  is just a scaled value of CSR\*. The reason for this is because the damping and shear modulus factors in Eq. (5) [i.e.,  $D_{\gamma c}$  and  $G_{\text{max}}(G/G_{\text{max}})_{\gamma c}$ ] are not constants, but vary as a function of the induced shear strain,  $\gamma_c$ , which in turn will be a function of the imposed shear stress, stiffness of the soil, shear stress-shear strain response of the soil, and so on. The relationship between  $\Delta W/\sigma'_{vo}$  and CSR\* is illustrated in Fig. 4, which shows  $\Delta W_1$  plotted as a function of CSR for varying soil densities and confining stresses. The significance of the non-oneto-one relationship between the two IMs is discussed subsequently in the context of the influence of effective confining stress and aging on liquefaction triggering.

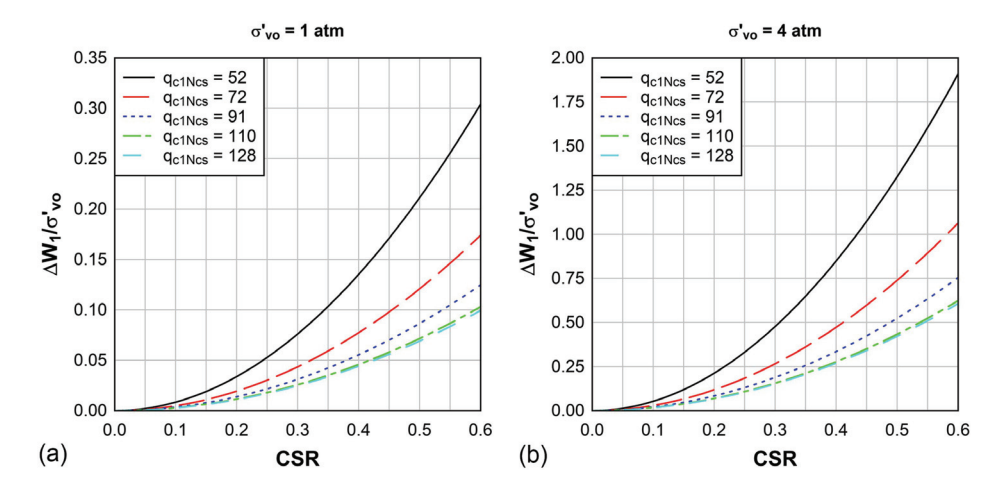


Fig. 4. Relationship between  $\Delta W_1$  and CSR for a range of soil densities and for initial vertical effective confining stress,  $\sigma'_{vo}$ , of (a) 100 kPa (~1 atm); and (b) 400 kPa (~4 atm). The vertical scale of the two plots is different.

#### **Ground Motion Duration**

As stated in the "Introduction," in simplified stress-based triggering models, the influence of the duration of the loading is accounted for via MSF, which is a function of  $n_{eq,M}$  normalized by  $n_{eq,M7.5}$ , where  $n_{eq,M7.5}$  is the duration of a reference earthquake having a M7.5 expressed in terms of number of equivalent cycles. In contrast,  $\Delta W$  directly accounts for the duration of the loading by integrating the shear stress-shear strain hysteresis loops for the duration of ground shaking. However, for the simplified implementation of the proposed energy-based triggering model, the duration of the loading is accounted for via a proposed  $n_{eq,M}$  relationship [i.e., Eq. (7)]. This same  $n_{eq,M}$  relationship was used by Green et al. (2019) to develop a MSF relationship for their proposed stressbased simplified procedure. However, in contrast to other  $n_{eq,M}$ relationships used to develop MSF for stress-based triggering models, Eq. (7) is a function of  $a_{\text{max}}$ , as well as M. Accordingly, a reference value of  $a_{\text{max}}$  is required, which Green et al. (2019) selected as 0.35g based review of the liquefaction case history databases. Nevertheless, the duration of the ground motion on liquefaction triggering is consistently accounted for in the simplified stressbased triggering model proposed by Green et al. (2019) and the simplified energy-based triggering model proposed herein.

#### Normalization of $\Delta W$ for Effective Confining Stress

In the proposed energy-based model,  $\Delta W$  is normalized by  $\sigma'_{vo}$  to account for the influence of initial effective confining stress on liquefaction triggering based on the findings of Lasley (2015) and Ulmer (2019). Of most significance, Ulmer (2019) performed cyclic simple shear tests on similar samples with vertical effective confining stresses 60, 100, and 250 kPa, and a unique correlation between  $(\Delta W_{\rm tot}/\sigma'_{vo})_{\rm liq}$  and  $D_r$  was shown to exist. This implies that the additional normalization for effective confining stress from  $K_\sigma$  used in computing CSR\* is inherently accounted for in  $\Delta W/\sigma'_{vo}$ . This is a direct result of  $\Delta W$  being a function of the induced shear strain,  $\gamma_c$ , which in turn is a function of the imposed shear stress, stiffness of the soil, shear stress—shear strain response of the soil, and so on.

In this vein, the imposed shear stress required to result in the same value of  $\Delta W_1/\sigma'_{vo}$  in similar samples confined at different initial effective confining stresses can be used to compute the  $K_\sigma$  relationship inherent to the proposed energy-based triggering model. As an example, the  $K_\sigma$  back-calculated by equating the normalized dissipated energies in two similar specimens having densities corresponding to  $q_{c1Ncs}=105$ , with one specimen confined at  $\sigma'_{vo}=100$  kPa (~1 atm) and the other at varying  $\sigma'_{vo}$  is shown if Fig. 5. The back-calculated values of  $K_\sigma$  shown in this figure are for FS $_L=1$ , where the CRR\* of the soil was estimated using the relationship proposed by Green et al. (2019).

Opposed to  $K_{\sigma}$ , the influence of initial effective confining stress inherent to the proposed energy-based triggering model is applied to imposed loading,  $\Delta W/\sigma'_{vo}$ , not to the ability of the soil to resist liquefaction  $(\Delta W/\sigma'_{vo})_{\rm liq}$ . The argument for this was articulated by Green et al. (2022), based on liquefaction triggering being a strain phenomenon, not a stress phenomenon, and as a result, the influence of effective confining stress on liquefaction triggering varies as a function of the FS $_L$ , among other factors. In addition to the back-calculated  $K_{\sigma}$  relationship from the proposed energy-based model, Fig. 5 also shows  $K_{\sigma}$  relationship used by Idriss and Boulanger (2008) and the  $K_{\gamma}$  relationship proposed by Green et al. (2022) assuming FS $_L=1$ .

As may be observed from this figure, the  $K_{\sigma}$  inherent to the proposed energy-based model plots lower than the other relationships, although it is not too different from the  $K_{\gamma}$  relationship proposed by Green et al. (2022). However, all the relationships shown

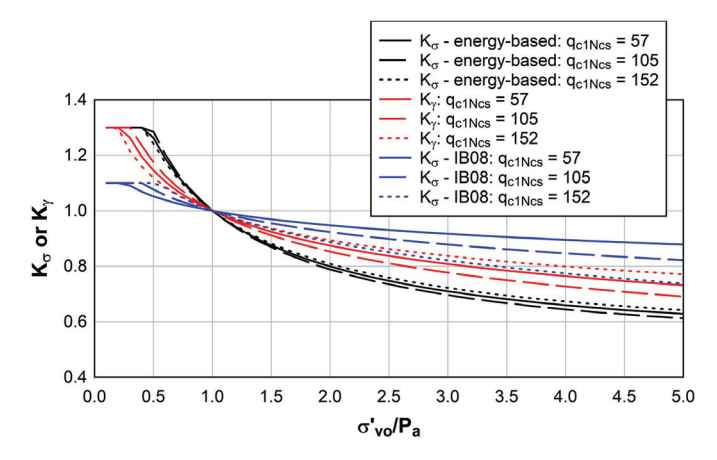


**Fig. 5.** Comparison of the  $K_{\sigma}$  relationship inherent in the proposed energy-based triggering model, the  $K_{\gamma}$  relationship proposed by Green et al. (2022), and the  $K_{\sigma}$  relationship used by Idriss and Boulanger (2008) (IB08) for three different soil densities.

in Fig. 5 lie within the range of scatter of laboratory determined values of  $K_{\sigma}$ .

#### Aging

The age of a soil deposit soil has been long recognized as having an influence on its susceptibility to liquefaction triggering (e.g., Youd and Hoose 1977), where the soil fabric changes with the age of the deposit, generally resulting in an increased resistance to liquefaction triggering. Seed (1979) proposed an early method for accounting for aging on liquefaction resistance by computing the ratio of the CRR of an aged soil to that of a young deposit of the same soil

$$K_{\rm DR} = \frac{\rm CRR_{aged}}{\rm CRR_{young}} \tag{25}$$

where  $K_{\rm DR}$  = liquefaction strength gain factor due to aging effects. However, Andrus et al. (2009) and Hayati and Andrus (2009) have shown that the time since last disturbance is more relevant to liquefaction triggering susceptibility than geologic age. The two are the same only if the deposit has not been significantly disturbed since deposition (e.g., if liquefaction has not been triggered in the deposit during a previous earthquake). Bwambale and Andrus (2019) developed the most recent relationship, at least that the authors are aware of, for  $K_{\rm DR}$  as a function of time by regressing compiled soil aging case histories

$$K_{\rm DR} = 0.13 \cdot \log(t) + 0.82 \tag{26}$$

where t = time since last major disturbance (years).

To estimate time since last disturbance, Andrus et al. (2009) proposed using the ratio of measured to estimated  $V_S$  (MEVR):

$$MEVR = \frac{Vs_{\text{measured}}}{Vs_{\text{estimated}}}$$
 (27)

where  $Vs_{\rm measured}$  is directly measured, and the estimated  $V_S$  (i.e.,  $Vs_{\rm estimated}$ ) is determined using correlations relating  $V_S$  and penetration resistance [e.g., Eq. (8)]. The underlying premise of the Andrus et al. (2009) approach is that the measurement of penetration resistance mobilizes intermediate to large strains that inherently disturb the soil fabric and, thus, is not that sensitive to aging effects (i.e., penetration resistance correlates to the  $V_S$  of the soil, if the soil were young, regardless of the time since last disturbance). In contrast, the measurement of  $V_S$  directly in the soil is

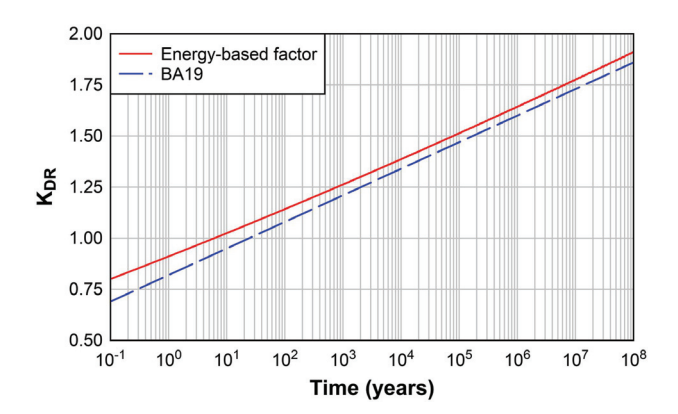


**Fig. 6.** Comparison of the aging liquefaction strength gain factor relationships inherent to the proposed energy-based triggering model and that proposed by Bwambale and Andrus (2019) (BA19).

a small-strain measurement and is sensitive to aging effects (i.e., it is the  $V_S$  of the aged soil). Thus, the ratio of directly measured  $V_S$  to that estimated from penetration resistance should be able to serve as an index for the time since last disturbance. In this vein, Andrus et al. (2009) developed the following correlation relating MEVR and t:

$$MEVR = 0.082 \cdot \log(t) + 0.935 \tag{28}$$

where t is in years.

As with  $K_{\sigma}$ , an inherent characteristic of  $\Delta W$  being a function of the induced shear strain,  $\gamma_c$ , is that the proposed energy-based triggering model accounts for the influence of soil aging on lique-faction triggering. An equivalent  $K_{\rm DR}$  relationship can be back-calculated from the proposed energy-based triggering model by using Eqs. (27) and (28) to estimate the  $G_{\rm max}$  for an aged soil. This can be done by taking the ratio of the shear stresses required to result in the same values of  $\Delta W$  in the aged and young sand. A comparison of the back-calculated  $K_{\rm DR}$  relationship and that proposed by Bwambale and Andrus (2019) [i.e., Eq. (26)] is shown in Fig. 6.

As may be observed from this figure, the two relationships are in excellent agreement. However, as opposed to  $K_{\rm DR}$ , the accounting for aging effects inherent to the proposed energy-based triggering

model is applied to imposed loading,  $\Delta W/\sigma'_{vo}$ , not to the ability of the soil to resist liquefaction  $(\Delta W/\sigma'_{vo})_{\rm liq}$  (i.e., aged soils have higher  $G_{\rm max}$ , and therefore for a given imposed shear stress, the induced  $\gamma_c$  is less and the  $\Delta W$  is less). As with the accounting for the influence of initial effective confining stress, the argument for this was articulated by Green et al. (2022), based on liquefaction triggering being a strain phenomenon, not a stress phenomenon, and as a result, the influence of aging effects on liquefaction triggering varies as a function of the FS<sub>L</sub>, among other factors.

#### **Initial Static Shear Stress**

In the simplified stress-based triggering models, the influence of initial static shear stress acting on a horizontal plane on liquefaction triggering is accounted for by the inclusion of the  $K_{\alpha}$  factor. The authors hypothesize that the influence of this initial static shear stress is also inherent to the proposed energy-based model. However, this would require the computation of  $\Delta W$  using modified Masing rules (e.g., Pyke 1979), for example, to account for the change in the shear stress—shear strain hysteretic behavior of the soil. At this time, the authors have not developed a simplified approach for computing  $\Delta W$  using the modified Masing rules as a function of  $\alpha$  (i.e., initial static shear stress acting on a horizontal plan normalized by the initial vertical effective stress).

Furthermore, and more importantly, the authors have not validated their hypothesis that the influence of initial static shear stress is inherent to the proposed energy-based model using laboratory data. Although these are planned future efforts in furthering the development of the energy-based triggering model, in the interim, the authors have developed energy-based  $K_{\alpha}$  relationships,  $K_{\alpha \_ \Delta W}$ , from the stress-based  $K_{\alpha}$  relationship used by Idriss and Boulanger (2008), where  $K_{\alpha \_ \Delta W}$  is given by

$$K_{\alpha - \Delta W} = \frac{\left(\frac{\Delta W}{\sigma_{vo}^{\prime}}\right)_{\text{liq} - \alpha}}{\left(\frac{\Delta W}{\sigma_{vo}^{\prime}}\right)_{\text{liq} - \alpha = 0}} \tag{29}$$

The resulting  $K_{\alpha_-\Delta W}$  relationships are presented in Fig. 7 for two initial effective confining stresses, with plots for initial effective confining stresses ranging from 100 to 1,000 kPa (1 to 10 atm) provided in Fig. S5. As may be surmised from Eq. (29),  $K_{\alpha_-\Delta W}$  is applied to the ability of the soil to resist liquefaction [i.e.,  $(\Delta W/\sigma'_{vo})_{\text{liq}}$ ] similar to how  $K_{\alpha}$  is implemented in the simplified stress-based models, and not to the imposed loading (i.e.,  $\Delta W/\sigma'_{vo}$ ) as would be the case if the

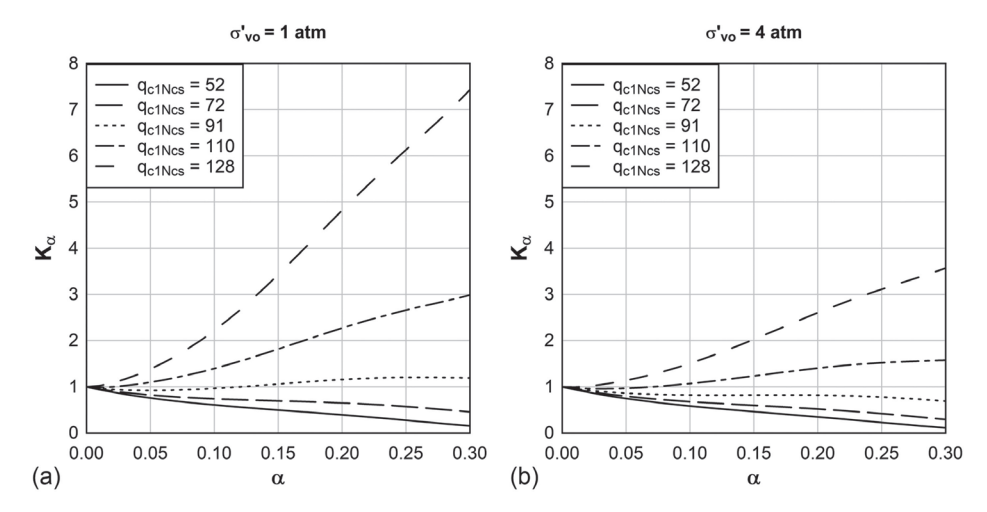


Fig. 7. Correction factors for initial static shear stress,  $K_{\alpha \Delta W}$ , computed from the  $K_{\alpha}$  relationships used by Idriss and Boulanger (2008) (IB08) for initial vertical effective confining stresses of (a) 100 kPa (~1 atm); and (b) 400 kPa (~4 atm).

modified Masing criteria were used to account for initial static shear stress.

# Comparison with the Boulanger and Idriss (2016) Triggering Model

Two simplified stress-based liquefaction evaluation procedures that use the original BI14 database as their basis are compared with the proposed energy-based procedure. These stress-based procedures use CSR\* to quantify the seismic loading (Boulanger and Idriss 2016; Green et al. 2019). Fig. 8 shows how the median ( $P_L = 50\%$ ) stress-based limit-state curves fit the data in CSR\* versus  $q_{c1Ncs}$  space compared with how the median proposed energy-based limit-state curve fits the data in  $\Delta W/\sigma'_{vo}$  versus  $q_{c1Ncs}$  space. The stress-based CSR\* values were computed using the data in the original BI14 database (from which these procedures were regressed) and values of  $\Delta W/\sigma'_{vo}$  were computed using the data in the updated database outlined in the Supplemental Materials. As a result, some of the noted trends may relate to the differences in the databases underlying the models.

Table 4 summarizes the number of correct predictions, false positives, and false negatives using the median curve from each procedure. False positives indicate that the procedure predicted

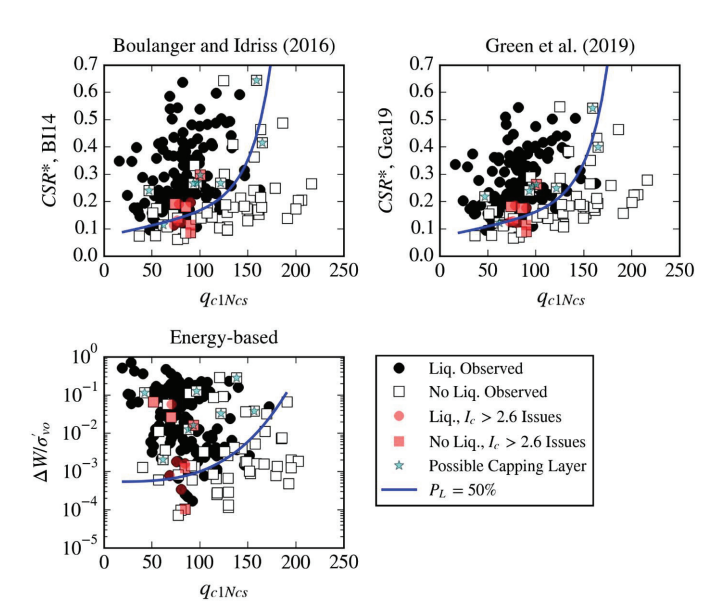


**Fig. 8.** Case histories common to the BI14 database and the updated database plotted as CSR\* versus  $q_{c1Ncs}$  for stress-based procedures and as normalized dissipated energy versus  $q_{c1Ncs}$  for the proposed energy-based method. Solid lines represent median ( $P_L = 50\%$ ) limit-state curves when uncertainties in input parameters are ignored. Non-black coloring and stars indicate case histories with potential issues that affect their accuracy.

**Table 4.** Number of correct, false positive, and false negative predictions for the proposed energy-based procedure and two stress-based procedures

Procedure	Correct	False positive	False negative
Energy-based, uncertainties excluded	193	36	23
Energy-based, uncertainties included	192	37	23
Boulanger and Idriss (2016)	204	23	25
Green et al. (2019)	207	23	22

liquefaction despite no observations of liquefaction manifestation at the site, and false negatives indicate that the procedure predicted no liquefaction despite observations of liquefaction manifestations at the site. The proposed energy-based method had nearly the same number of correct predictions as the two stress-based methods, but the ratio of false positives to false negatives was higher.

It is expected that there would be false negative predictions because the lack of surficial manifestations of liquefaction does not necessarily indicate that liquefaction was not triggered at depth (e.g., Upadhyaya et al. 2022). There are several potential issues that could prevent surficial manifestations, such as a thick unsaturated crust at the surface or thick layers of soil with high plasticity, i.e.,  $I_c$  greater than 2.6 (Green et al. 2018). Nine No liquefaction case histories were identified as having this issue and are marked as having a possible capping layer in Fig. 8.

Another confounding issue could be interbedded layers of soil with  $I_c > 2.6$  within the critical layer (Maurer et al. 2014, 2015; Upadhyaya et al. 2018; Cubrinovski et al. 2019). Eleven case histories with this issue are also marked in Fig. 8. These case histories were not removed from the database because of these issues; however, it is important to note that such issues exist and may affect the accuracy of these evaluation procedures when such issues are present. If these were excluded, then the ratio of false positive to false negative predictions given in Table 4 would be closer to unity.

It is emphasized, however, that the comparisons presented in Fig. 8 and Table 4 only represent data from a narrow range of scenarios [e.g., earthquake magnitude, depth to liquefaction, and so on (NRC 2016)]. Greater differences between the stress- and energy-based procedures likely exist for scenarios different from those represented by the case history database.

#### **Conclusions**

The objective of this research was to develop an energy-based model for evaluating liquefaction triggering. Normalized dissipated energy per unit volume of soil captures both the amplitude and duration of the ground shaking, to include the variation of the amplitude of the motion throughout the duration of shaking and the soil response, and is mechanistically linked to excess porewater pressure generation. In its simplified form, the proposed energy-based model is implemented similarly to the simplified stress-based models, with the only additional inputs required relative to stress-based models being soil stiffness and shear modulus reduction and damping (MRD) curves. The additional information resulting from introduction of soil stiffness and MRD curves inherently merges aspects of the stress- and strain-based liquefaction triggering concepts into one model, where liquefaction is inherently a strain phenomenon.

However, use of normalized dissipated energy as the IM circumvents issues with quantifying the ground motion duration inherent to simplified strain-based procedures. The energy-based limit-state curves derived herein using maximum likelihood regression have comparable predictive ability to stress-based limit-state curves in terms of number of correct predictions. As with existing stress-based limit-state curves based on similar case history databases of predominantly nonplastic sands and silty sands, the limit-state curves derived herein are limited to these soil types and may not be applicable for soils with plastic fines or with significant fines content.

The proposed energy-based model has desirable implementation scalability and applicability characteristics. Specifically,

refinements can be made to the imposed loading on the soil and to the soil's ability to resist liquefaction triggering. These refinements can be made by using soil-, site- or region-specific relationships/values in computing the imposed seismic loading or by performing site-specific site response analyses (i.e., nonsimplified implementation of the model). Additionally, refinements to the ability of the soil to resist liquefaction triggering can be made by performing undrained cyclic tests on undisturbed samples. Details on how to determine the normalized dissipated energy per unit volume of soil within a total stress framework were presented.

The use of IMs common to other earthquake engineering analyses that are consistent with seismic hazard maps issued by regulators, the implementation scalability characteristics of the proposed model, and/or the consistent operation within a total stress framework separate the proposed model from previously proposed energy-based triggering models. Additionally, the mechanistic robustness of the chosen IM is given further credence because it inherently accounts certain aspects of the influence of initial effective confining stress and aging effects on liquefaction triggering, which need to be accounted for by additional relationships when other IMs are used.

Because dissipated energy is a fundamental engineering metric, the applicability of the proposed model is broader than that of simplified stress-based models. Within the realm of earthquake analyses, the model can be used to analyze liquefaction triggering for free-field sites, to include liquefaction triggering of aged soils using directly measured values of  $V_S$  to compute  $G_{\text{max}}$ . Also, because dissipated energy is a scalar quantity, multidirectional shaking and other effects such as soil-structure interaction, nonvertical wave fields, and topographic site effects can readily be accounted for. Furthermore, the model can be used to analyze flow liquefaction of earthen dams, for example, resulting from earthquake shaking using a hybrid total stress/effective stress approach. Use of dissipated energy as the cumulative damage metric in these analyses is more direct than applying stress-based cycle counting methods, which are currently used. Inherently, not linking the duration of the ground vibrations to earthquake magnitude broadens the applicability of the model to nonearthquake-type applications. As a result, the proposed model can be used to evaluate, for example, liquefaction due to construction vibrations.

# **Data Availability Statement**

Some or all data, models, or code that support the findings of this paper are available from the corresponding author upon reasonable request.

### **Acknowledgments**

This study is based on work supported in part by the National Science Foundation (NSF) Grant Nos. CMMI-1435494, CMMI-1825189, and CMMI-1937984. The authors gratefully acknowledge this support; however, any opinions, findings, and conclusions or recommendations expressed in this paper are those of the authors and do not necessarily reflect the views of NSF. The authors would like to thank Dr. Sam Lasley for his work (Lasley 2015) on which this study builds. The authors also gratefully acknowledge Dr. Brett Maurer for providing many of the digitized CPT soundings and geographic coordinates for case histories in the database and Dr. Sneha Upadhyaya for providing updated  $a_{\rm max}$  values for the Darfield and Christchurch events.

# **Supplemental Materials**

Table S1 and Figs. S1–S5 are available online in the ASCE Library (www.ascelibrary.org).

#### References

- Andrus, R. D., H. Hayati, and N. P. Mohanan. 2009. "Correcting liquefaction resistance for aged sands using measured to estimated velocity ratio." *J. Geotech. Geoenviron. Eng.* 135 (6): 735–744. https://doi.org/10.1061/(ASCE)GT.1943-5606.0000025.
- Beaty, M. H., and P. M. Byrne. 2008. "Liquefaction and deformation analyses using a total stress approach." *J. Geotech. Geoenviron. Eng.* 134 (8): 1059–1072. https://doi.org/10.1061/(ASCE)1090-0241(2008) 134:8(1059).
- Berrill, J. B., and R. O. Davis. 1985. "Energy dissipation and seismic lique-faction of sands: Revised model." Soils Found. 25 (2): 106–118. https://doi.org/10.3208/sandf1972.25.2\_106.
- Boore, D. M., and T. Kishida. 2017. "Relations between some horizontal-component ground-motion intensity measures used in practice." Bull. Seismol. Soc. Am. 107 (1): 334–343. https://doi.org/10.1785/0120160250
- Boulanger, R. W., and I. M. Idriss. 2014. CPT and SPT based liquefaction triggering procedures. Rep. No. UCD/CGM-14/01. Davis, CA: Univ. of California.
- Boulanger, R. W., and I. M. Idriss. 2016. "CPT-based liquefaction triggering procedure." *J. Geotech. Geoenviron. Eng.* 142 (2): 04015065. https://doi.org/10.1061/(ASCE)GT.1943-5606.0001388.
- Bradley, B. 2013. "Site-specific and spatially-distributed ground-motion intensity estimation in the 201–2011 Canterbury earthquakes." Soil Dyn. Earthquake Eng. 61 (Jun): 3–91. https://doi.org/10.1016/j.soildyn .2014.01.025.
- Brandenberg, S. J., et al. 2020. "Next-generation liquefaction database." *Earthquake Spectra* 36 (2): 939–959. https://doi.org/10.1177/8755293 020902477.
- Bullock, Z., S. Dashti, A. B. Liel, K. A. Porter, and B. W. Maurer. 2022. "Probabilistic liquefaction triggering and manifestation models based on cumulative absolute velocity." *J. Geotech. Geoenviron. Eng.* 148 (3): 04021196. https://doi.org/10.1061/(ASCE)GT.1943-5606 .0002729.
- Bwambale, B., and R. D. Andrus. 2019. "State of the art in the assessment of aging effects on soil liquefaction." *Soil Dyn. Earthquake Eng.* 125 (Oct): 105658. https://doi.org/10.1016/j.soildyn.2019.04.032.
- Cetin, K. O., A. Der Kiureghian, and R. B. Seed. 2002. "Probabilistic models for the initiation of seismic soil liquefaction." *Struct. Saf.* 24 (1): 67–82. https://doi.org/10.1016/S0167-4730(02)00036-X.
- Cetin, K. O., R. B. Seed, R. E. Kayen, R. E. S. Moss, H. T. Bilge, M. Ilgac, and K. Chowdhury. 2018. "SPT-based probabilistic and deterministic assessment of seismic soil liquefaction triggering hazard." Soil Dyn. Earthquake Eng. 115 (Dec): 698–709. https://doi.org/10.1016/j.soildyn.2018.09.012.
- Cubrinovski, M., A. Rhodes, N. Ntritsos, and S. Van Ballegooy. 2019. "System response of liquefiable deposits." *Soil Dyn. Earthquake Eng.* 124 (Sep): 212–229. https://doi.org/10.1016/j.soildyn.2018.05.013.
- Darendeli, M. B. 2001. "Development of a new family of normalized modulus reduction and material damping curves." Ph.D. dissertation, Dept. of Civil, Architectural, and Environmental Engineering, Univ. of Texas at Austin.
- Davis, R. O., and J. B. Berrill. 2001. "Pore pressure and dissipated energy in earthquakes—Field verification." *J. Geotech. Geoenviron. Eng.* 127 (3): 269–274. https://doi.org/10.1061/(ASCE)1090-0241(2001) 127:3(269).
- Dobry, R., R. S. Ladd, F. Y. Yokel, R. M. Chung, and D. Powell. 1982. Prediction of pore water pressure buildup and liquefaction of sands during earthquakes by the cyclic strain method: Building science series. Washington, DC: National Bureau of Standards.
- Figueroa, J. L., A. S. Saada, L. Liang, and N. M. Dahisaria. 1994. "Evaluation of soil liquefaction by energy principles." *J. Geotech. Eng.*

- 120 (9): 1554–1569. https://doi.org/10.1061/(ASCE)0733-9410(1994) 120:9(1554).
- Franke, K. W., and S. M. Olson. 2021. "Practical considerations regarding the probability of liquefaction in engineering design." J. Geotech. Geoenviron. Eng. 147 (8): 04021061. https://doi.org/10.1061/(ASCE)GT .1943-5606.0002561.
- Geyin, M., B. W. Maurer, B. A. Bradley, R. A. Green, and S. van Ballegooy. 2021. "CPT-based liquefaction case histories compiled from three earthquakes in Canterbury, New Zealand." *Earthquake Spectra* 37 (4): 2920–2945. https://doi.org/10.1177/8755293021996367.
- Green, R. A. 2001. "Energy-based evaluation and remediation of liquefiable soils." Ph.D. dissertation, Dept. of Civil and Environmental Engineering, Virginia Tech.
- Green, R. A., J. J. Bommer, A. Rodriguez-Marek, B. W. Maurer, P. J. Stafford, B. Edwards, P. P. Kruiver, G. de Lange, and J. van Elk. 2019. "Addressing limitations in existing 'simplified' liquefaction triggering evaluation procedures: Application to induced seismicity in the Groningen gas field." *Bull. Earthquake Eng.* 17 (8): 4539–4557. https://doi.org/10.1007/s10518-018-0489-3.
- Green, R. A., A. Bradshaw, and C. D. P. Baxter. 2022. "Accounting for intrinsic soil properties and state variables on liquefaction triggering in simplified procedures." *J. Geotech. Geoenviron. Eng.* 148 (7): 04022056. https://doi.org/10.1061/(ASCE)GT.1943-5606.0002823.
- Green, R. A., M. Cubrinovski, B. Cox, C. Wood, L. Wotherspoon, B. Bradley, and B. Maurer. 2014. "Select liquefaction case histories from the 2010–2011 Canterbury earthquake sequence." *Earthquake Spectra* 30 (1): 131–153. https://doi.org/10.1193/030713EQS066M.
- Green, R. A., B. W. Maurer, and S. van Ballegooy. 2018. "The influence of the non-liquefied crust on the severity of surficial liquefaction manifestations: Case history from the 2016 Valentine's Day earthquake in New Zealand." In Geotechnical earthquake engineering and soil dynamics V, liquefaction triggering, consequences, and mitigation, 21–32. Reston, VA: ASCE.
- Green, R. A., and J. K. Mitchell. 2003. "A closer look at arias intensity-based liquefaction evaluation procedures." In *Proc.*, 7th Pacific Conf. on Earthquake Engineering. Christchurch, New Zealand: Univ. of Canterbury.
- Green, R. A., and J. K. Mitchell. 2004. "Energy-based evaluation and remediation of liquefiable soils." In *Geo-Trans 2004: Geotechnical Engineering for Transportation Projects*, Geotechnical Special Publication 223, edited by M. K. Yegian and E. Kavazanjian, 1961–1970. Reston, VA: ASCE.
- Green, R. A., and J. K. Mitchell. 2010. "Comparison of energies required to densify liquefiable soil." In Proc., 5th Int. Conf. Recent Advances in Geotechnical Earthquake Engineering and Soil Dynamics and Symp. in Honor of Professor I.M. Idriss. Rolla, MO: Missouri Univ. of Science and Technology.
- Green, R. A., J. K. Mitchell, and C. P. Polito. 2000. "An energy-based excess pore pressure generation model for cohesionless soils." In *Proc.*, *John Booker Memorial Symp. Developments in Theoretical Geomechanics*, edited by D. W. Smith and J. P. Carter, 383–390. Rotterdam, Netherlands: A.A. Balkema.
- Green, R. A., and E. Rodriguez-Arriaga. 2019. "Assessment of an alternative implementation of the Dobry et al. cyclic strain procedure for evaluating liquefaction triggering." In *Proc.*, 7th Int. Conf. on Earthquake Geotechnical Engineering (7ICEGE). London: International Society for Soil Mechanics and Geotechnical Engineering.
- Green, R. A., and G. A. Terri. 2005. "Number of equivalent cycles concept for liquefaction evaluations—Revisited." J. Geotech. Geoenviron. Eng. 131 (4): 477–488. https://doi.org/10.1061/(ASCE)1090-0241(2005) 131:4(477).
- Hayati, H., and R. D. Andrus. 2009. "Updated liquefaction resistance correlation factors for aged sands." *J. Geotech. Geoenviron. Eng.* 135 (11): 1683–1692. https://doi.org/10.1061/(ASCE)GT.1943-5606.0000118.
- Hryciw, R. D., S. Vitton, and T. G. Thomann. 1990. "Liquefaction and flow failure during seismic exploration." *J. Geotech. Eng.* 116 (12): 1881– 1899. https://doi.org/10.1061/(ASCE)0733-9410(1990)116:12(1881).
- Idriss, I. M., and R. W. Boulanger. 2008. Soil liquefaction during earth-quakes. Monograph MNO-12. Oakland, CA: Earthquake Engineering Research Institute.

- Idriss, I. M., and J. I. Sun. 1992. User's manual for SHAKE91: A computer program for conducting equivalent linear seismic site response analyses of horizontally layered soil deposits. Davis, CA: Univ. of California.
- Ishibashi, I., and X. Zhang. 1993. "Unified dynamic shear moduli and damping ratios of sand and clay." Soils Found. 33 (1): 182–191. https:// doi.org/10.3208/sandf1972.33.182.
- Jacobsen, L. S. 1930. "Steady forced vibration as influenced by damping: An approximate solution of the steady forced vibration of a system of one degree of freedom under the influence of various types of damping." *Trans. Am. Soc. Mech. Eng.* 52 (2): 169–181. https://doi.org/10.1115/1 .4057368.
- Jafarian, Y., I. Towhata, M. H. Baziar, A. Noorzad, and A. Bahmanpour. 2012. "Strain energy based evaluation of liquefaction and residual pore water pressure in sands using cyclic torsional shear experiments." Soil Dyn. Earthquake Eng. 35 (Apr): 13–28. https://doi.org/10.1016/j .soildyn.2011.11.006.
- Kayen, R., R. E. S. Moss, E. M. Thompson, R. B. Seed, K. O. Cetin, A. Der Kiureghian, Y. Tanaka, and K. Tokimatsu. 2013. "Shear-wave velocitybased probabilistic and deterministic assessment of seismic soil liquefaction potential." *J. Geotech. Geoenviron. Eng.* 139 (3): 407–419. https://doi.org/10.1061/(ASCE)GT.1943-5606.0000743.
- Kayen, R. E., and J. K. Mitchell. 1997. "Assessment of liquefaction potential during earthquakes by arias intensity." J. Geotech. Geoenviron. Eng. 123 (12): 1162–1174. https://doi.org/10.1061/(ASCE)1090-0241 (1997)123:12(1162).
- Kokusho, T., and Y. Kaneko. 2018. "Energy evaluation for liquefaction-induced strain of loose sands by harmonic and irregular loading tests." Soil Dyn. Earthquake Eng. 114 (Nov): 362–377. https://doi.org/10.1016/j.soildyn.2018.07.012.
- Kokusho, T., and S. Tanimoto. 2021. "Energy capacity versus liquefaction strength investigated by cyclic triaxial tests on intact soils." *J. Geotech. Geoenviron. Eng.* 147 (4): 04021006. https://doi.org/10.1061/(ASCE) GT.1943-5606.0002484.
- Kramer, S. L., and R. A. Mitchell. 2006. "Ground motion intensity measures for liquefaction hazard evaluation." *Earthquake Spectra* 22 (2): 413–438. https://doi.org/10.1193/1.2194970.
- Lamens, P., and A. Askarinejad. 2021. "Pile driving and submarine slope stability: A hybrid engineering approach." *Landslides* 18: 1351–1367. https://doi.org/10.1007/s10346-020-01585-2.
- Lasley, S. J. 2015. "Application of fatigue theories to seismic compression estimation and the evaluation of liquefaction potential." Ph.D. dissertation, Dept. of Civil and Environmental Engineering, Virginia Tech.
- Lasley, S. J., R. A. Green, and A. Rodriguez-Marek. 2016. "New stress reduction coefficient relationship for liquefaction triggering analyses." J. Geotech. Geoenviron. Eng. 142 (11): 06016013. https://doi.org/10.1061/(ASCE)GT.1943-5606.0001530.
- Lasley, S. J., R. A. Green, and A. Rodriguez-Marek. 2017. "Number of equivalent stress cycles for liquefaction evaluations in active tectonic and stable continental regimes." *J. Geotech. Geoenviron. Eng.* 143 (4): 04016116. https://doi.org/10.1061/(ASCE)GT.1943-5606.0001629.
- Lee, K. L., and H. B. Seed. 1967. "Cyclic stress conditions causing lique-faction of sands." J. Soil Mech. Found. Div. 93 (1): 47–70. https://doi.org/10.1061/JSFEAQ.0000945.
- Luco, N., and C. A. Cornell. 2007. "Structure-specific scalar intensity measures for near-source and ordinary earthquake ground motions." *Earthquake Spectra* 23 (2): 357–392. https://doi.org/10.1193/1.2723158.
- Martin, G. R., W. D. L. Finn, and H. B. Seed. 1975. "Fundamentals of liquefaction under cyclic loading." *J. Geotech. Eng. Div.* 101 (5): 423–438. https://doi.org/10.1061/AJGEB6.0000164.
- Maurer, B. W., R. A. Green, M. Cubrinovski, and B. A. Bradley. 2014. "Evaluation of the liquefaction potential index for assessing liquefaction hazard in Christchurch, New Zealand." *J. Geotech. Geoenviron. Eng.* 140 (7): 04014032. https://doi.org/10.1061/(ASCE)GT.1943-5606.0001117.
- Maurer, B. W., R. A. Green, M. Cubrinovski, and B. A. Bradley. 2015. "Fines-content effects on liquefaction hazard evaluation for infrastructure in Christchurch, New Zealand." Soil Dyn. Earthquake Eng. 76 (3): 58–68. https://doi.org/10.1016/j.soildyn.2014.10.028.

- Menq, F.-Y. 2003. "Dynamic properties of sandy and gravelly soils." Ph.D. dissertation, Dept. of Civil, Architectural, and Environmental Engineering, Univ. of Texas at Austin.
- Moss, R. E. S. 2003. "CPT-based probabilistic assessment of seismic soil liquefaction initiation." Ph.D. dissertation, Dept. of Civil and Environmental Engineering, Univ. of California.
- Moss, R. E. S., R. B. Seed, R. E. Kayen, J. P. Stewart, A. Der Kiureghian, and K. O. Cetin. 2006. "CPT-based probabilistic and deterministic assessment of in situ seismic soil liquefaction potential." *J. Geotech. Geoenviron. Eng.* 132 (8): 1032–1051. https://doi.org/10.1061/(ASCE) 1090-0241(2006)132:8(1032).
- Naesgaard, E., and P. M. Byrne. 2007. "Flow liquefaction simulation using a combined effective stress—Total stress model." In *Proc.*, 60th Canadian Geotechnical Conf. Ottawa: Canadian Geotechnical Society.
- Nemat-Nasser, S., and A. Shokooh. 1979. "A unified approach to densification and liquefaction of cohesionless sand in cyclic shearing." *Can. Geotech. J.* 16 (4): 659–678. https://doi.org/10.1139/t79-076.
- NRC (National Research Council). 2016. State of the art and practice in the assessment of earthquake-induced soil liquefaction and its consequences. Committee on earthquake induced soil liquefaction assessment (Edward Kavazanjian, Jr., Chair, Jose E. Andrade, Kandian "Arul" Arulmoli, Brian F. Atwater, John T. Christian, Russell A. Green, Steven L. Kramer, Lelio Mejia, James K. Mitchell, Ellen Rathje, James R. Rice, and Yumie Wang). Washington, DC: NRC.
- Ostadan, F., N. Deng, and I. Arango. 1998. "Energy-based method for liquefaction potential evaluation." In Proc., 11th European Conf. on Earthquake Engineering. Rotterdam, Netherlands: A.A. Balkema.
- Peck, R. B. 1979. "Liquefaction potential: Science versus practice." J. Geotech. Eng. Div. 105 (3): 393–398. https://doi.org/10.1061/AJGEB6.0000776.
- Polito, C., R. A. Green, E. Dillon, and C. Sohn. 2013. "The effect of load shape on the relationship between dissipated energy and residual excess pore pressure generation in cyclic triaxial tests." *Can. Geotech. J.* 50 (11): 1118–1128. https://doi.org/10.1139/cgj-2012-0379.
- Polito, C. P., R. A. Green, and J. Lee. 2008. "Pore pressure generation models for sands and silty soils subjected to cyclic loading." *J. Geotech. Geoenviron. Eng.* 134 (10): 1490–1500. https://doi.org/10.1061/(ASCE)1090-0241(2008)134:10(1490).
- Pyke, R. 1979. "Nonlinear soil models for irregular cyclic loading." J. Geotech. Eng. Div. 105 (6): 715–726. https://doi.org/10.1061/AJGEB6.0000820.
- Riemer, M. F., W. B. Gookin, J. D. Bray, and I. Arango. 1994. Effects of loading frequency and control on the liquefaction behavior of clean sands. Rep. No. UCB/GT/94-07. Berkeley, CA: Univ. of California.
- Rodriguez-Arriaga, E., and R. A. Green. 2018. "Assessment of the cyclic strain approach for evaluating liquefaction triggering." Soil Dyn. Earthquake Eng. 113 (Oct): 202–214. https://doi.org/10.1016/j.soildyn.2018 .05.033.
- Rodriguez-Marek, A., E. M. Rathje, J. J. Bommer, F. Scherbaum, and P. J. Stafford. 2014. "Application of single-station sigma and site-response characterization in a probabilistic seismic-hazard analysis for a new nuclear site." *Bull. Seismol. Soc. Am.* 104 (4): 1601–1619. https://doi.org/10.1785/0120130196.
- Seed, H. B. 1979. "Soil liquefaction and cyclic mobility evaluation for level ground during earthquakes." J. Geotech. Eng. Div. 105 (2): 201–255. https://doi.org/10.1061/AJGEB6.0000768.

- Seed, H. B. 1983. "Earthquake resistant design of earth dams." In *Proc.*, Symp. on Seismic Design of Embankments and Caverns, 41–64. Reston, VA: ASCE.
- Seed, H. B., and I. M. Idriss. 1971. "Simplified procedure for evaluating soil liquefaction potential." J. Soil Mech. Found. Div. 97 (9): 1249–1273. https://doi.org/10.1061/JSFEAQ.0001662.
- Simcock, K. J., R. O. Davis, J. B. Berrill, and G. Mullenger. 1983. "Cyclic triaxial tests with continuous measurement of dissipated energy." *Geotech. Test. J.* 6 (1): 35–39. https://doi.org/10.1520/GTJ10822J.
- Taylor, O.-D. S. 2011. "Use of energy-based liquefaction approach to predict deformation in silts due to pile driving." Ph.D. dissertation, Dept. of Civil and Environmental Engineering, Univ. of Rhode Island.
- Thum, T. S., S. Lasley, R. A. Green, and A. Rodriguez-Marek. 2019. ShakeVT2: A computer program for equivalent linear site response analysis. Center for Geotechnical Practice and Research (CGPR) Rep. #98. Blacksburg, VA: The Charles E. Via, Jr., Department of Civil and Environmental Engineering, Virginia Tech.
- Ulmer, K. J. 2019. "Development of an energy-based liquefaction evaluation procedure." Ph.D. dissertation, Dept. of Civil and Environmental Engineering, Virginia Tech.
- Ulmer, K. J., R. A. Green, and A. Rodriguez-Marek. 2020. "A consistent correlation between V<sub>S</sub>, SPT, and CPT metrics for use in liquefaction evaluation procedures." In *Geo-Congress 2020: Geotechnical Earth-quake Engineering and Special Topics*, Geotechnical Special Publication 318, edited by J. P. Hambleton, R. Makhnenko, and A. S. Budge, 132–140. Reston, VA: ASCE.
- Upadhyaya, S. 2019. "Development of an improved and internally-consistent framework for evaluating liquefaction damage potential." Ph.D. dissertation, Dept. of Civil and Environmental Engineering, Virginia Tech.
- Upadhyaya, S., R. A. Green, A. Rodriguez-Marek, and B. W. Maurer. 2022.
  "True liquefaction triggering curve." J. Geotech. Geoenviron. Eng. 149 (3): 04023005. https://doi.org/10.1061/JGGEFK.GTENG-11126.
- Upadhyaya, S., B. W. Maurer, R. A. Green, and A. Rodriguez-Marek. 2018. "Effect of non-liquefiable high fines-content, high plasticity soils on liquefaction potential index (LPI) performance." In *Geotechnical Earthquake Engineering and Soil Dynamics V: Liquefaction Triggering, Consequences, and Mitigation*, Geotechnical Special Publication 290, edited by S. J. Brandenberg and M. T. Manzari, 191–198. Reston, VA: ASCE.
- USGS. 2019. "ShakeMap." Accessed September 12, 2019. https://earthquake.usgs.gov/data/shakemap/.
- Wair, B. R., J. T. Dejong, and T. Shantz. 2012. Guidelines for estimation of shear wave velocity profiles. Rep. No. 2012/08. Berkeley, CA: Univ. of California.
- Yee, E., J. P. Stewart, and K. Tokimatsu. 2013. "Elastic and large-strain nonlinear seismic site response from analysis of vertical array recordings." J. Geotech. Geoenviron. Eng. 139 (10): 1789–1801. https://doi .org/10.1061/(ASCE)GT.1943-5606.0000900.
- Youd, T. L., and S. N. Hoose. 1977. "Liquefaction susceptibility and geologic setting." In *Proc.*, 6th World Conf. on Earthquake Engineering, 2189–2194. Tokyo: International Association for Earthquake Engineering.
- Zeghal, M., and A.-W. Elgamal. 1994. "Analysis of site liquefaction using earthquake records." *J. Geotech. Eng.* 120 (6): 996–1017. https://doi.org/10.1061/(ASCE)0733-9410(1994)120:6(996).
- Zimmaro, P., et al. 2019. "Next-generation liquefaction." *Earthquake Spectra* 36 (2): 939–959. https://doi.org/10.1177/8755293020902477.